VSP

Advanced Robotics 22 (2008) 949–981

ADVANCED ROBOTICS
www.brill.nl/ar

Full paper

Dynamic Analysis of a Macro–Micro Redundantly Actuated Parallel Manipulator

Hamid D. Taghirad [a,*] **and Meyer A. Nahon** [b]

[a] Advanced Robotics and Automated Systems, Department of Electrical Engineering, K. N. Toosi University of Technology, PO Box 16315-1355, Tehran, Iran

[b] Center for Intelligent Machines, Department of Mechanical Engineering, McGill University, Montréal, Quebec, Canada H3A 2K6

Received 2 November 2007; accepted 15 January 2008

Abstract

In this paper the dynamic analysis of a macro–micro parallel manipulator is studied in detail. The manipulator architecture is a simplified planar version adopted from the structure of the Large Adaptive Reflector (LAR), the Canadian design of next-generation giant radio telescopes. In this structure it is proposed to use two parallel redundant manipulators at the macro and micro level, both actuated by cables. In this paper, the governing dynamic equation of motion of such a structure is derived using the Newton–Euler formulation. Next, the dynamic equations of the system are used in the open-loop inverse dynamics simulations, as well as closed-loop forward dynamics simulations. In the open-loop dynamic simulations it is observed that the inertial forces of the limbs contribute only 10% of the dynamic forces required to generate a typical trajectory and, moreover, the total dynamic forces contribute only 10% of the experimentally measured disturbance forces. Furthermore, in the closed-loop simulations using decentralized PD controllers at the macro and micro levels, it is shown that the macro–micro structure results in a 10 times more accurate positioning than that in the first stage of the macro–micro structure. This convincing result promotes the use of the macro–micro structure for LAR application.

Keywords

Parallel manipulator, dynamics analysis, inverse kinematics, Jacobian, acceleration analysis, Newton–Euler formulation, macro–micro robot, PD control

1. Introduction

An international consortium of radio astronomers and engineers has agreed to investigate technologies to build the Square Kilometer Array (SKA), a centimeter-to-meter wave radio telescope for the next generation of investigation into cosmic

* To whom correspondence should be addressed. E-mail: taghirad@kntu.ac.ir

 DOI:10.1163/156855308X315145

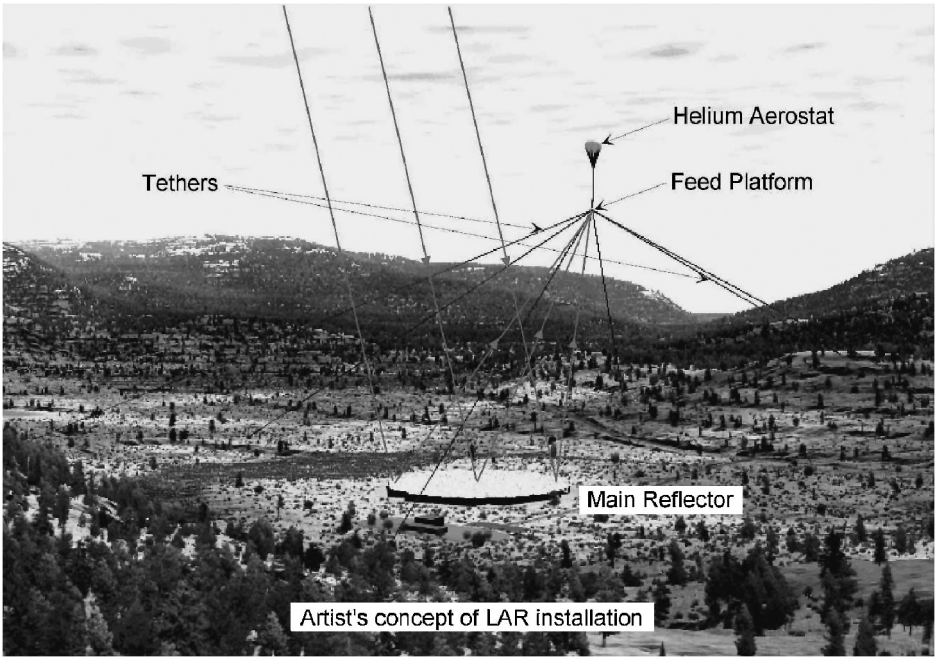

Figure 1. An artist's concept of a complete 200-m diameter LAR installation.

phenomena [1–3]. A looming 'sensitivity barrier' will prevent current telescopes from making much deeper inroads at these wavelengths, particularly in studies of the early universe. The Canadian proposal for the SKA design consists of an array of 30–50 individual antennas whose signals are combined to yield the resolution of a much larger antenna. Each of these antennas would use the Large Adaptive Reflector (LAR) concept put forward by a group led by the National Research Council of Canada, and supported by university and industry collaborators [4–6]. The LAR design is applicable to telescopes up to several hundred meters in diameter. However, design and construction of a 200-m LAR prototype is pursued by the National Research Council of Canada. Figure 1 is an artist's concept of a complete 200-m diameter LAR installation, which consists of two central components. The first is a 200-m diameter parabolic reflector with a focal length of 500 m, composed of actuated panels supported by the ground. The second component is the receiver package which is supported by a tension structure consisting of multiple long tethers and a helium-filled aerostat as shown schematically in Fig. 2. With funding from the Canada Foundation for Innovation, a one-third scale prototype of the multi-tethered aerostat subsystem has been designed and implemented in Penticton [7]. It should be noted that even at one third scale, this system is very large, with a footprint of roughly 1 km^2.

The challenging problem in this system is accurately positioning the feed (receiver) in the presence of disturbances, such as wind turbulence. For the positioning

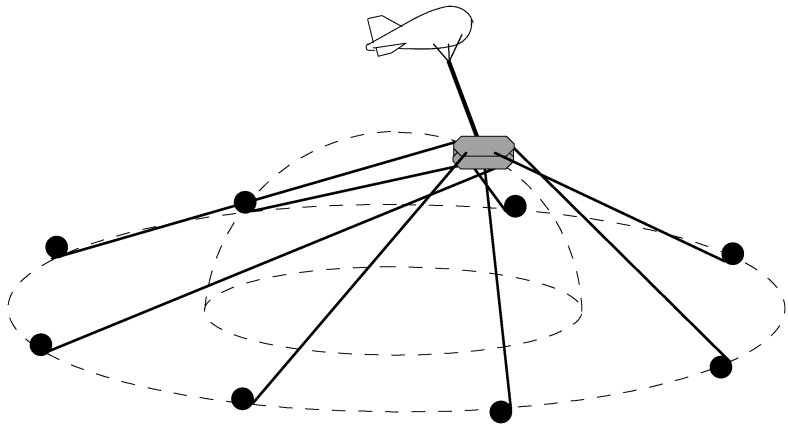

Figure 2. Schematics of the LCM with eight cables and aerostat.

structure of the receiver a macro–micro manipulator design is proposed, in which at both the macro and micro levels two redundantly actuated cable-driven parallel manipulators are used. As illustrated in Fig. 2, at the macro level the receiver is moved to various locations on a circular hemisphere and its positioning is controlled by changing the lengths of eight tethers with ground winches. The cable-driven macro manipulator used in this design, which is called the Large Cable Mechanism (LCM), is in fact a 6-d.o.f. cable-driven redundantly actuated manipulator. For sufficient coverage of the sky, the LCM must be capable of positioning the receiver for a wide range of zenith angles ($0 \leqslant \theta_z \leqslant 60°$) and for the full range of azimuth angles ($0 \leqslant \theta_a \leqslant 360°$). Once the receiver is in place, the position controller of the system at the micro level responds to disturbances such as wind gusts in order to limit the movement of the receiver to centimeter accuracy. At this level a Confluence Point Mechanism (CPM) is designed to perform the final small-scale corrections at high frequencies. The CPM requires 6 d.o.f. and is also a redundantly actuated cable-driven parallel manipulator. The CPM base is attached to the LCM structure with tethers and its moving platform accurately positions the telescope feed (receiver). This design is intended to keep the moving platform of the CPM, and hence the feed, as close to stationary as possible, and pointed toward the center of the reflector.

Since in the design of the LCM/CPM a macro–micro structure is proposed in which at each level a redundantly actuated parallel manipulator is used for extreme positioning accuracy, this paper intends to study the dynamic analysis of such macro–micro structures in detail. Although the analysis of the above system is naturally adopted from the design of the LCM/CPM structure, it touches two leading topics in parallel robotics research, i.e., tendon-driven redundant parallel manipulators and macro/micro structure in parallel structures, which have their own merits and potential application beyond the LAR. In the LCM/CPM structure, two parallel manipulators with 6 d.o.f. are used at the macro and micro levels. In contrast to the

open-chain macro–micro manipulator, the dynamic analysis of parallel manipulators with such structures exhibits an inherent complexity, due to their closed loops and kinematic constraints. Therefore, in order to keep the analysis complexity at a managable level, while preserving all the important analysis elements, a simplified version of the macro–micro structure is considered in this paper as the basis of the analysis. This structure is composed of two parallel 4RPR mechanisms, both actuated by cables. In this simplified structure, although a planar version of the mechanisms is considered, two important features of the original design, i.e., the cable-driven actuators with redundancy for each subsystem and the macro–micro structure of the original design, are employed.

In contrast to the open-chain serial manipulators, the dynamic modeling of parallel manipulators presents an inherent complexity due to their closed-loop structure and kinematic constraints. Nevertheless, the dynamic modeling is quite important for the control, particularly because parallel manipulators are preferred in applications where precise positioning and good dynamic performance under high load are the prime requirements. In recent years, there has been a great amount of research on the kinematics of parallel manipulators, but works on the dynamics of parallel manipulators are relatively few. Several approaches have been proposed for the dynamic analysis of parallel manipulators. The traditional Newton–Euler formulation is used for the dynamic analysis of general parallel manipulators [8] and also for the Stewart platform, which is the most celebrated parallel manipulator [9]. In this formulation the equation of motion for each limb and the moving platform must be derived, which inevitably leads to a large number of equations and less computational efficiency. On the other hand, all the reaction forces can be computed, which is very useful in the design of a parallel manipulator. The Lagrangian formulation eliminates all the unwanted reaction forces at the outset, and it is more efficient [10]. However, because of the numerous constraints imposed by the closed loops of a parallel manipulator, deriving explicit equations of motion in terms of a set of independent generalized coordinates becomes a prohibitive task [11]. A third approach is to use the principle of virtual work, in which the computation of the constraint forces is bypassed [12]. In this method the inertial forces and moments are computed using the linear and angular accelerations of each of the bodies. Then, the whole manipulator is considered to be in static equilibrium and the principle of virtual work is applied to derive the input force or torque [12]. Since constraint forces and moments do not need to be computed, this approach leads to faster computational algorithms, which is an important advantage for the purposes of control of a manipulator [13]. Other approaches have also been suggested in the literature [14, 15]. Inverse dynamic formulations are used primarily for the closed-loop control algorithms applied for parallel manipulators. Among the reported research, a position control routine using inverse dynamics of Stewart platform is implemented in Ref. [16], while stiffness control for such manipulator is implemented in Ref. [11]. Among the many control topologies reported in the

literature, the dynamics and control of redundantly actuated parallel manipulators has been considered by fewer researchers [17].

Due to the potential attraction of the macro–micro structure in the LAR application, a thorough analysis on the kinematics and dynamics of the described macro–micro parallel manipulator has been developed, and some-closed loop control topologies are proposed and simulated for this system. The governing dynamic equation of motion of the macro–micro manipulator is derived using both the Newton–Euler formulation and the principle of virtual work Newton–Euler formulation. In this paper the dynamic analysis of this system using the Newton–Euler formulation is reported, while the virtual work method is presented in Ref. [18]. Furthermore, the dynamic equations of the system are used in two sets of simulations. First, the inverse dynamic simulations are presented, in which the required actuator torques to generate a predefined trajectory is computed. It is shown that for a typical trajectory, the limb inertial forces contributes only 10% of the dynamic forces and the total dynamic forces contribute only 10% of external forces in the presence of some experimentally measured disturbance forces. Finally, the inverse dynamic equations are used in a special implicit integration routine in order to simulate the dynamic behavior of the system in closed-loop form and in the presence of disturbances. It is shown that for a typical trajectory and in the presence of experimentally measured disturbance forces, the macro–micro structure results in 10 times more accurate positioning than that in the first stage of the macro–micro structure. This convincing result promotes the use of the macro–micro structure in the LAR application.

2. Mechanism Description

The architecture of the planar macro–micro 2×4RPR parallel manipulator considered for our studies is shown in Fig. 3. This manipulator consists of two similar 4RPR parallel structures at the macro and micro level. At each level the moving platform is supported by four limbs of identical kinematic structure. At the macro level each limb connects the fixed base to the macro manipulator moving platform by a revolute joint (R) followed by a prismatic joint (P) and another revolute joint (R). The kinematic structure of a prismatic joint is used to model the elongation of each cable-driven limb. In order to avoid singularities at the central position of the manipulator at each level, the cable-driven limbs are considered to be crossed. Complete kinematic and singularity analysis of the mechanism is reported in Ref. [21]. At the micro level a similar 4RPR structure is used; however, the base points of the macro manipulators are located on the moving platform of the macro manipulator. Angular positions of fixed base and moving platform attachment points are given in Table 1, in which capital letters are used to describe the macro manipulator variables, while small letters are used for that of the micro manipulator. In this presentation, A_i denotes the fixed base points of the limbs, B_i denotes the connection points of the limbs on the moving platform, L_i denotes the limb lengths and

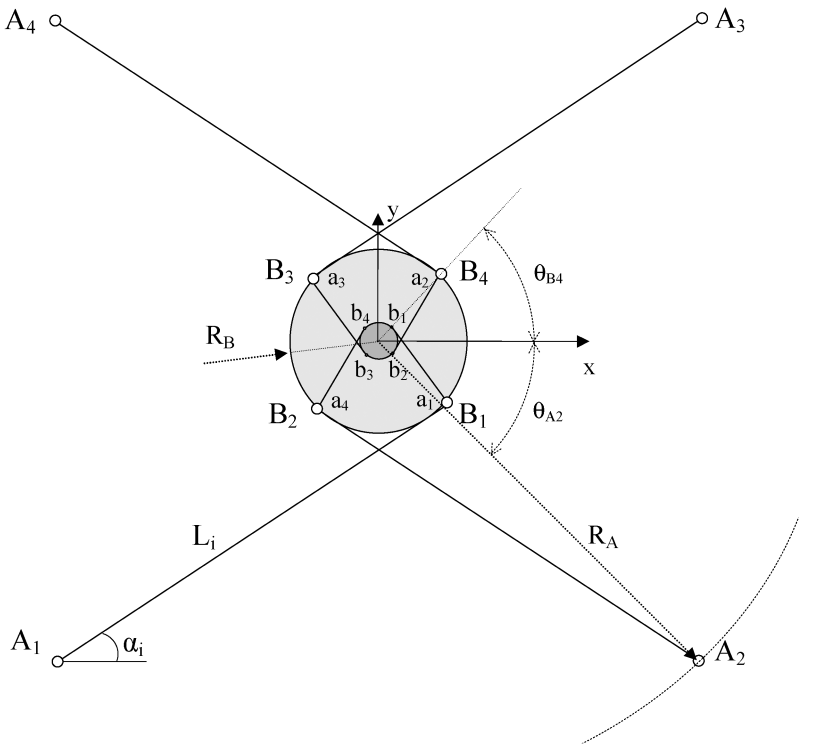

Figure 3. Schematics of the 2 × 4RPR mechanism employed for the analysis of the LCM/CPM structure.

α_i denotes the limb angles. The position of the center of the moving platform at the macro level is denoted by $G = [x_G, y_G]$ and the final position of the micro manipulator g is denoted by $g = [x_g, y_g]$, which both are measured relative to the inertial coordinate frame depicted in Figs 3 and 4. The absolute orientation of the macro manipulator moving platform is denoted by ϕ and the absolute orientation of the micro manipulator with respect to the fixed coordinate frame is denoted by ψ.

The planar structure used in this analysis is a simplified version of the LCM/CPM design, in which the two important features of the main mechanism, i.e., the macro–micro structure and actuator redundancy, are preserved in a planar structure. Although in the simplified structured used in this analysis, the 6 d.o.f. of the real system is down scaled to 3 d.o.f. and the vertical motion of the feed is neglected, the dynamic analysis results can be used to verify the significance of the macro–micro structure in the design. The control objective in the simplified mechanism is to track the desired position and orientation of the final micro moving platform in the presence of a disturbance force, such as wind turbulence. The geometry of the fixed and moving platform attachment points, A_i, B_i, a_i and b_i, are considered to be arbitrary in the analysis and they are not necessarily coincident. However, the parameter used in the simulations of the system is adopted from the LCM/CPM design and is symmetrical, as given in Table 1.

Table 1.
Geometric and inertial parameters of macro–micro manipulator according to the LCM/CPM design

Description	Symbols	Quantity
Location circle radius of the macro fixed points A_i	R_A	900 m
Location circle radius of the macro moving points B_i	R_B	10 m
Location circle radius of the micro base points a_i	R_a	10 m
Location circle radius of the micro moving points b_i	R_b	2 m
Angle of macro fixed points A_i	θ_{A_i}	$[-135°, -45°, 45°, 135°]$
Angle of macro moving points B_i	θ_{B_i}	$[-45°, -135°, 135°, 45°]$
Angle of micro fixed points a_i	θ_{a_i}	$[-45°, 45°, 135°, -135°]$
Angle of micro moving points b_i	θ_{b_i}	$[45°, -45°, -135°, 135°]$
Macro moving platform mass	M	2500 kg
Macro moving platform moment of inertia	I_M	3.5×10^5 kg · m^2
Macro limb density per length	ρ_M	0.215 kg/m
Micro moving platform mass	m	500 kg
Micro moving platform moment of inertia	I_m	2×10^3 kg · m^2
Micro limb density per length	ρ_m	0.1 kg/m
Maximum macro actuator force	$\tau_{A_{\max}}$	5 kN
Maximum micro actuator force	$\tau_{a_{\max}}$	50 N

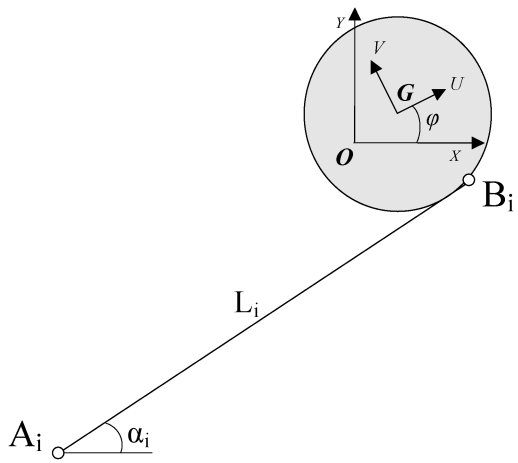

Figure 4. Kinematics configuration of the macro manipulator.

3. Kinematic Analysis

3.1. Position Analysis

In this section, the kinematic of the system is detailed. In this analysis the inverse kinematics of the macro manipulator is analyzed first and then the kinematic analysis of the macro–micro assembly is presented.

3.1.1. Inverse Kinematics of the Macro Manipulator

For the inverse kinematic analysis of the macro manipulator, it is assumed that the position and orientation of the moving platform $\mathbf{X} = [x_G, y_G, \phi]^{\mathrm{T}}$ is given and the problem is to find the joint variable of the macro manipulator, $\mathbf{L} = [L_1, L_2, L_3, L_4]^{\mathrm{T}}$. For the purpose of analysis and as it is illustrated in Fig. 3, a fixed frame $O:xy$ is attached to the fixed base at the point O, the center of the circle which passes through A_i's, and another moving coordinate frame $G:UV$ is attached to the macro manipulator moving platform at point G. Furthermore, assume that the point A_i lies at the radial distance of R_A from point O and the point B_i lies at the radial distance of R_B from point G in the xy-plane, when the manipulator is at the central location.

In order to specify the geometry of the macro manipulator define $\theta_{A_i}, \theta_{B_i}$ as the absolute angle of the points A_i and B_i at the central configuration of the macro manipulator, with respect to the fixed frame O. Moreover, notice that the moving platform experiences a position and orientation of $[x_G, y_G, \phi]^{\mathrm{T}}$ at each instant. Let us define the instantaneous orientation angle of B_i as:

$$\phi_i = \phi + \theta_{B_i}. \tag{1}$$

Therefore, for each limb, $i = 1, 2, \ldots, 4$, the position of the base points, A_i are given by:

$$A_i = [R_A \cos(\theta_{A_i}), R_A \sin(\theta_{A_i})]^{\mathrm{T}}. \tag{2}$$

From the geometry of the macro manipulator as illustrated in Fig. 4, the loop-closure equation for each limb, $i = 1, 2, \ldots, 4$, can be written as:

$$\overrightarrow{A_i G} = \overrightarrow{A_i B_i} + \overrightarrow{B_i G}. \tag{3}$$

Rewriting the vector loop closure component-wise:

$$x_G - x_{A_i} = L_i \cos(\alpha_i) - R_B \cos(\phi_i) \tag{4}$$

$$y_G - y_{A_i} = L_i \sin(\alpha_i) - R_B \sin(\phi_i), \tag{5}$$

in which α_i is the absolute limb angles. To solve the inverse kinematic problem, α_i must be eliminated from the above equation and it must be rewritten in terms of L_i. This can be accomplished by reordering the above equation as:

$$L_i \cos(\alpha_i) = x_G - x_{A_i} + R_B \cos(\phi_i) \tag{6}$$

$$L_i \sin(\alpha_i) = y_G - y_{A_i} + R_B \sin(\phi_i). \tag{7}$$

By adding the square of both sides of (6) and (7) the limb lengths are uniquely determined:

$$L_i = \left[\left(x_G - x_{A_i} + R_B \cos(\phi_i)\right)^2 + \left(y_G - y_{A_i} + R_B \sin(\phi_i)\right)^2\right]^{1/2}. \tag{8}$$

Furthermore, the limb angles α_i can be determined from:

$$\alpha_i = \operatorname{atan2}\left[\left(y_G - y_{A_i} + R_B \sin(\phi_i)\right), \left(x_G - x_{A_i} + R_B \cos(\phi_i)\right)\right]. \tag{9}$$

Hence, corresponding to each given macro manipulator location $\mathbf{X} = [x_G, y_G, \phi]^{\mathrm{T}}$, there is a unique solution for the limb length L_i and limb angle α_i.

3.1.2. Macro–Micro Kinematics

For inverse kinematic analysis of the macro–micro manipulator, it is assumed that the position and orientation of the macro moving platform $\mathbf{X} = [x_G, y_G, \phi]^{\mathrm{T}}$ and that of the micro moving platform $\mathbf{x} = [x_g, y_g, \psi]^{\mathrm{T}}$ are given. The problem is then to find the joint variables of the macro manipulator, $\mathbf{L} = [L_1, L_2, L_3, L_4]^{\mathrm{T}}$ and that of the micro manipulator $\boldsymbol{\ell} = [\ell_1, \ell_2, \ell_3, \ell_4]^{\mathrm{T}}$, respectively. As explained before capital letters are reserved for the macro manipulator variables, while small letters are used to denote micro manipulator variables.

For the purpose of the analysis and as illustrated in Fig. 4, in addition to the frame $O:xy$ which is attached to the fixed base at the point O and the macro moving coordinate frame $G:UV$ attached to the macro manipulator at point G, consider the micro moving coordinate frame $g:uv$ which is attached to the micro manipulator moving platform at point g, the center of the micro moving platform. Furthermore, assume that the points a_i lie at the radial distance of R_a from point G and the points b_i lie at the radial distance of R_b from point g in the uv plane. In order to specify the geometry of the macro manipulator, as illustrated in Fig. 5 in addition to the definition of $\theta_{A_i}, \theta_{B_i}$, define $\theta_{a_i}, \theta_{b_i}$ as the absolute angle of the points a_i and b_i at the central configuration of the macro manipulator, with respect to the fixed frame O. Moreover, notice that the micro moving platform experiences a position and orientation of $[x_g, y_g, \psi]^{\mathrm{T}}$ at each instant as it is shown in Fig. 5.

Since the structures of the macro and micro manipulators are the same, the inverse kinematic solution of the macro–micro system is similar to that of the macro manipulator and can be found in the following sequence. Starting with the macro manipulator inverse kinematic solution, for a given $\mathbf{X} = [x_G, y_G, \phi]^{\mathrm{T}}$, the macro joint variables L_i and α_i are determined from (8) and (9), respectively. Then

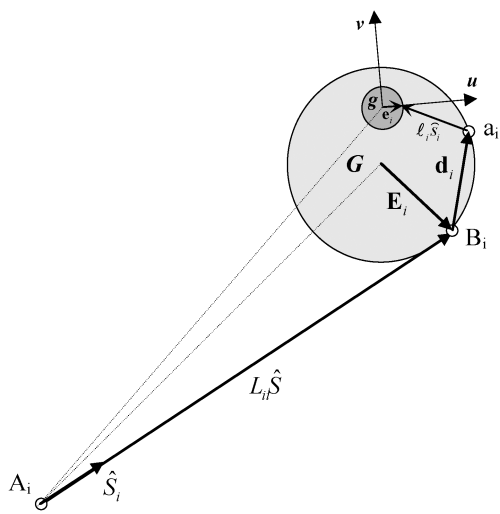

Figure 5. Vector definitions for the Jacobian derivation of the macro manipulator.

the coordinates of points B_i and a_i are determined from the following geometrical relation:

$$B_i = [x_G + R_B \cos(\theta_{B_i} + \phi),\, y_G + R_B \sin(\theta_{B_i} + \phi)]^{\mathrm{T}} \tag{10}$$

$$a_i = [x_G + R_a \cos(\theta_{a_i} + \phi),\, y_G + R_a \sin(\theta_{a_i} + \phi)]^{\mathrm{T}}. \tag{11}$$

Finally, assuming that the micro manipulator position and orientation $[x_g, y_g, \psi]^{\mathrm{T}}$ are given, the micro manipulator joint variables can be determined by the following equations, similar to that of the macro manipulator equations (8) and (9):

$$\ell_i = \left[\left(x_g - x_{a_i} + R_b \cos(\psi_i)\right)^2 + \left(y_g - y_{a_i} + R_b \sin(\psi_i)\right)^2\right]^{1/2}, \tag{12}$$

in which:

$$\psi_i = \psi + \theta_{b_i}. \tag{13}$$

Furthermore, the micro manipulator limb angles β_i can be determined from:

$$\beta_i = \operatorname{atan2}\left[\left(y_g - y_{a_i} + R_b \sin(\psi_i)\right), \left(x_g - x_{a_i} + R_b \cos(\psi_i)\right)\right]. \tag{14}$$

3.2. Jacobian Analysis

Jacobian analysis plays a vital role in the study of robotic manipulators. The Jacobian matrix not only reveals the relation between the joint variable velocities $\dot{\mathbf{L}}$ and the moving platform velocities $\dot{\mathbf{X}}$, it constructs the transformation needed to find the actuator forces $\boldsymbol{\tau}$ from the forces acting on the moving platform $\mathbf{F}$. In this section the Jacobian analysis for the macro manipulator is performed first and then the Jacobian matrix of the macro–micro manipulator is derived.

3.2.1. Macro Jacobian

Contrary to the serial manipulators, the Jacobian matrix of a parallel manipulator is defined as the transformation matrix that converts the moving platform velocities to the joint variable velocities, i.e.:

$$\dot{\mathbf{L}} = \mathbf{J}_M \cdot \dot{\mathbf{X}}. \tag{15}$$

In which, for the macro manipulator $\dot{\mathbf{L}} = [\dot{L}_1, \dot{L}_2, \dot{L}_3, \dot{L}_4]$ is the 4×1 limb velocity vector and $\dot{\mathbf{X}} = [\dot{x}_G, \dot{y}_G, \dot{\phi}]$ is the 3×1 moving platform velocity vector. Therefore, the macro Jacobian matrix $\mathbf{J}_M$ is a non-square 4×3 matrix. In order to obtain the Jacobian matrix, let us differentiate the vector loop equation (3) with respect to time, considering the vector definitions $\hat{\mathbf{S}}_i$ and $\mathbf{E}_i$ illustrated in Fig. 5. Hence, for $i = 1, 2, \ldots, 4$:

$$\mathbf{v}_G + \dot{\phi}(\hat{\mathbf{K}} \times \mathbf{E}_i) = \dot{L}_i \hat{\mathbf{S}}_i + \dot{\alpha}_i \dot{L}_i (\hat{\mathbf{K}} \times \hat{\mathbf{S}}_i). \tag{16}$$

In which, $\mathbf{v}_G = [\dot{x}_G, \dot{y}_G]^{\mathrm{T}}$ is the velocity of the moving platform at point G and $\hat{\mathbf{K}}$ is the unit vector along the Z-direction of the fixed coordinate frame O. Furthermore, the vectors $\mathbf{E}_i$ and $\hat{\mathbf{S}}_i$ can be found from the inverse kinematic relation by:

$$\hat{\mathbf{S}}_i = [\cos(\alpha_i), \sin(\alpha_i)]^{\mathrm{T}} \tag{17}$$

$$\mathbf{E}_i = [R_B \cos(\theta_{B_i} + \phi),\, R_B \sin(\theta_{B_i} + \phi)]^{\mathrm{T}}. \tag{18}$$

In order to eliminate $\dot{\alpha}_i$, dot multiply both sides of (16) by $\hat{\mathbf{S}}_i$:

$$\hat{\mathbf{S}}_i \cdot \mathbf{v}_G + \dot{\phi}\hat{\mathbf{K}}(\mathbf{E}_i \times \hat{\mathbf{S}}_i) = \dot{L}_i. \tag{19}$$

Rewriting (19) in a matrix form:

$$\dot{L}_i = [\, S_{ix} \mid S_{iy} \mid E_{ix}S_{iy} - E_{iy}S_{ix} \,] \cdot \begin{bmatrix} v_{Gx} \\ v_{Gy} \\ \dot{\phi} \end{bmatrix}. \tag{20}$$

Using (20) for $i = 1, 2, \ldots, 4$ the macro Jacobian matrix $\mathbf{J}_M$, which is a 4×3 matrix, is derived as follows:

$$\mathbf{J}_M = [\, S_{ix} \mid S_{iy} \mid E_{ix}S_{iy} - E_{iy}S_{ix} \,]_{i=1}^{4}. \tag{21}$$

In order to get an expression for $\dot{\alpha}_i$, cross-multiply both sides of (16) by $\hat{\mathbf{S}}_i$:

$$\hat{\mathbf{S}}_i \times \mathbf{v}_G + \dot{\phi}(\mathbf{E}_i \cdot \hat{\mathbf{S}}_i)\hat{\mathbf{K}} = \dot{\alpha}_i L_i \hat{\mathbf{K}}. \tag{22}$$

Rewriting the third component of (22) in matrix form:

$$\dot{\alpha}_i = \frac{1}{L_i} \cdot [\, -S_{iy} \mid S_{ix} \mid E_{ix}S_{ix} + E_{iy}S_{iy} \,] \cdot \begin{bmatrix} v_{Gx} \\ v_{Gy} \\ \dot{\phi} \end{bmatrix}. \tag{23}$$

Therefore, $\mathbf{J}_\alpha$ is defined as the matrix relating the vector of moving platform velocities, $\dot{\mathbf{X}} = [\dot{x}_G, \dot{y}_G, \dot{\phi}]$ to the vector of angular velocities of the limbs $\dot{\boldsymbol{\alpha}} = [\dot{\alpha}_1, \dot{\alpha}_2, \dot{\alpha}_3, \dot{\alpha}_4]$ as:

$$\dot{\boldsymbol{\alpha}} = \mathbf{J}_\alpha \cdot \dot{\mathbf{X}}, \tag{24}$$

in which:

$$\mathbf{J}_\alpha = \frac{1}{L_i} \cdot [\, -S_{iy} \mid S_{ix} \mid E_{ix}S_{ix} + E_{iy}S_{iy} \,]_{i=1}^{4}. \tag{25}$$

3.2.2. Macro–Micro Jacobian

As illustrated in Fig. 5 denote $\hat{\mathbf{s}}_i$ as the unit vector along the micro manipulator limb i, $\mathbf{e}_i$ the vector form the point g to b_i, and $\mathbf{d}_i$ as the vector from the point B_i to the point a_i. The vector loop closure for the micro manipulator can be written as:

$$\overrightarrow{A_i g} + \overrightarrow{g b_i} = \overrightarrow{A_i B_i} + \overrightarrow{B_i a_i} + \overrightarrow{a_i b_i}. \tag{26}$$

Substitute $\overrightarrow{A_i B_i}$ from (3):

$$\overrightarrow{A_i g} + \overrightarrow{g b_i} = \overrightarrow{A_i G} + \overrightarrow{G B_i} + \overrightarrow{B_i a_i} + \overrightarrow{a_i b_i}. \tag{27}$$

Differentiate both sides with respect to time:

$$\mathbf{v}_g + \dot{\psi}(\hat{\mathbf{K}} \times \mathbf{e}_i) = \mathbf{v}_G + \dot{\phi}(\hat{\mathbf{K}} \times \mathbf{E}_i) + \dot{\phi}(\hat{\mathbf{K}} \times \mathbf{d}_i) + \dot{\ell}_i \hat{\mathbf{s}}_i + \dot{\beta}_i \ell_i (\hat{\mathbf{K}} \times \hat{\mathbf{s}}_i), \tag{28}$$

in which $\hat{\mathbf{s}}_i$ and $\mathbf{d}_i$ are given from inverse kinematic relation by:

$$\hat{\mathbf{s}}_i = [\cos(\beta_i), \sin(\beta_i)]^{\mathrm{T}} \tag{29}$$

$$\mathbf{d}_i = R_a[\cos(\theta_{a_i} + \phi) - \cos(\theta_{B_i} + \phi), \sin(\theta_{a_i} + \phi) - \sin(\theta_{B_i} + \phi)]^{\mathrm{T}}. \tag{30}$$

Dot multiply both sides of (28) by $\hat{\mathbf{s}}_i$ to eliminate $\dot{\beta}$:

$$\hat{\mathbf{s}}_i \cdot \mathbf{v}_g + \dot{\psi}\hat{\mathbf{K}} \cdot (\mathbf{e}_i \times \hat{\mathbf{s}}_i) = \hat{\mathbf{s}}_i \cdot \mathbf{v}_G + \dot{\phi}\hat{\mathbf{K}} \cdot \big((\mathbf{E}_i + \mathbf{d}_i) \times \hat{\mathbf{s}}_i\big) + \dot{\ell}_i. \tag{31}$$

Rewriting (31) into matrix form:

$$\begin{aligned} &[\, s_{ix} \,|\, s_{iy} \,|\, e_{ix}s_{iy} - e_{iy}s_{ix} \,] \cdot \begin{bmatrix} v_{gx} \\ v_{gy} \\ \dot{\psi} \end{bmatrix} \\ &\quad = [\, s_{ix} \,|\, s_{iy} \,|\, (E_{ix} + d_{ix})s_{iy} - (E_{iy} + d_{iy})s_{ix} \,] \cdot \begin{bmatrix} v_{Gx} \\ v_{Gy} \\ \dot{\phi} \end{bmatrix} + \dot{\ell}_i. \end{aligned} \tag{32}$$

Using (32) for $i = 1, 2, \ldots, 4$ define two different Jacobian matrices $\mathbf{J}_m$, the micro manipulator Jacobian, and $\mathbf{J}_{M_m}$ as the macro–micro coupled Jacobian as:

$$\mathbf{J}_m = [\, s_{ix} \,|\, s_{iy} \,|\, e_{ix}s_{iy} - e_{iy}s_{ix} \,]_{i=1}^{4} \tag{33}$$

$$\mathbf{J}_{M_m} = [\, s_{ix} \,|\, s_{iy} \,|\, (E_{ix} + d_{ix})s_{iy} - (E_{iy} + d_{iy})s_{ix} \,]_{i=1}^{4}. \tag{34}$$

Hence:

$$\mathbf{J}_m \cdot \dot{\mathbf{x}} = \mathbf{J}_{M_m} \cdot \dot{\mathbf{X}} + \dot{\boldsymbol{\ell}}. \tag{35}$$

Equation (35) constitutes the relation between the micro manipulator joint velocity vector $\dot{\boldsymbol{\ell}}$ to the macro and micro cartesian space velocities $\dot{\mathbf{X}}$ and $\dot{\mathbf{x}}$. Moreover, the total macro–micro manipulator Jacobian matrix $\mathbf{J}_t$ can be defined as the projection matrix of total the macro–micro joint velocities $\dot{\boldsymbol{\mathcal{L}}} = [\dot{\mathbf{L}}, \dot{\boldsymbol{\ell}}]^{\mathrm{T}}$ to the vector of macro and micro moving platform velocities $\dot{\boldsymbol{\mathcal{X}}} = [\dot{\mathbf{X}}, \dot{\mathbf{x}}]^{\mathrm{T}}$ as:

$$\dot{\boldsymbol{\mathcal{L}}} = \mathbf{J}_t \cdot \dot{\boldsymbol{\mathcal{X}}}. \tag{36}$$

The Jacobian matrix $\mathbf{J}_t$ can be derived by grouping $\boldsymbol{\mathcal{L}}$ and $\boldsymbol{\mathcal{X}}$ from (15) and (35):

$$\mathbf{J}_t = \begin{bmatrix} \mathbf{J}_M & \mathbf{0} \\ -\mathbf{J}_{M_m} & \mathbf{J}_m \end{bmatrix}. \tag{37}$$

As seen from this equation the total Jacobian matrix of the macro–micro manipulator is a block triangular matrix, which contains the macro and micro individual Jacobian matrices $\mathbf{J}_M$ and $\mathbf{J}_m$ as the diagonal blocks and the coupling Jacobian matrix $\mathbf{J}_{M_m}$ as the off-diagonal block.

In order to get an expression for $\dot{\beta}_i$, cross-multiply both sides of (28) by $\hat{\mathbf{s}}_i$:

$$\hat{\mathbf{s}}_i \times \mathbf{v}_g + \dot{\psi}(\mathbf{e}_i \cdot \hat{\mathbf{s}}_i)\hat{\mathbf{K}} = \hat{\mathbf{s}}_i \times \mathbf{v}_G + \dot{\phi}\big((\mathbf{E}_i + \mathbf{d}_i) \cdot \hat{\mathbf{s}}_i\big)\hat{\mathbf{K}} + \dot{\beta}_i \ell_i \hat{\mathbf{K}}. \tag{38}$$

Rewriting (38) in matrix form:

$$\dot{\beta}_i = \frac{1}{\ell_i} \cdot [\, -s_{iy} \,|\, s_{ix} \,|\, e_{ix}s_{ix} + e_{iy}s_{iy} \,] \cdot \begin{bmatrix} v_{gx} \\ v_{gy} \\ \dot{\psi} \end{bmatrix} - \frac{1}{\ell_i} \cdot [\, -s_{iy} \,|\, s_{ix} \,|\, (E_{ix} + d_{ix})s_{ix} + (E_{iy} + d_{iy})s_{iy} \,] \cdot \begin{bmatrix} v_{Gx} \\ v_{Gy} \\ \dot{\phi} \end{bmatrix}. \quad (39)$$

3.3. Acceleration Analysis

Acceleration analysis of the limbs and the moving platform is needed for Newton–Euler formulation of a parallel manipulator. In this section the acceleration analysis for the macro manipulator is performed first and then the acceleration analysis of the macro–micro manipulator is derived.

3.3.1. Macro Accelerations

In acceleration analysis it is intended to derive expressions for the linear and angular accelerations of the limbs, i.e., $\ddot{L}_i$ and $\ddot{\alpha}_i$, as a function of the moving platform acceleration $\ddot{\mathbf{X}} = [\ddot{x}_G, \ddot{y}_G, \ddot{\phi}]^{\mathrm{T}}$. In order to obtain such a relation differentiate the vector loop equation (16) with respect to time, considering the vector definitions $\hat{\mathbf{S}}_i$ and $\mathbf{E}_i$ as given in (17) and (18), and illustrated in Fig. 5. Furthermore, note that $\dot{\hat{\mathbf{S}}}_i = \dot{\alpha}_i(\hat{\mathbf{K}} \times \hat{\mathbf{S}}_i)$ and $\dot{\mathbf{E}}_i = \dot{\phi}(\hat{\mathbf{K}} \times \mathbf{E}_i)$. Hence, for $i = 1, 2, \ldots, 4$:

$$\begin{aligned} &\mathbf{a}_G + \ddot{\phi}(\hat{\mathbf{K}} \times \mathbf{E}_i) - \dot{\phi}^2\mathbf{E}_i \\ &\quad = \ddot{L}_i\hat{\mathbf{S}}_i + 2\dot{L}_i\dot{\alpha}_i(\hat{\mathbf{K}} \times \hat{\mathbf{S}}_i) + \ddot{\alpha}_i L_i(\hat{\mathbf{K}} \times \hat{\mathbf{S}}_i) - \dot{\alpha}_i^2 L_i\hat{\mathbf{S}}_i. \end{aligned} \quad (40)$$

In order to eliminate $\ddot{\alpha}_i$ and get an expression for $\ddot{L}_i$, dot multiply both side by $\hat{\mathbf{S}}_i$ and reorder it into:

$$\ddot{L}_i = \mathbf{a}_G \cdot \hat{\mathbf{S}}_i + \ddot{\phi}\hat{\mathbf{K}}(\mathbf{E}_i \times \hat{\mathbf{S}}_i) - \dot{\phi}^2(\mathbf{E}_i \cdot \hat{\mathbf{S}}_i) + \dot{\alpha}_i^2 L_i. \quad (41)$$

In order to eliminate $\ddot{L}_i$ and get an expression for $\ddot{\alpha}_i$, cross-multiply both sides of 40 by $\hat{\mathbf{S}}_i$:

$$\hat{\mathbf{S}}_i \times \mathbf{a}_G + \ddot{\phi}(\mathbf{E}_i \cdot \hat{\mathbf{S}}_i)\hat{\mathbf{K}} - \dot{\phi}^2(\hat{\mathbf{S}}_i \times \mathbf{E}_i) = (2\dot{L}_i\dot{\alpha}_i + \ddot{\alpha}_i L_i)\hat{\mathbf{K}}. \quad (42)$$

This simplifies to:

$$\ddot{\alpha}_i = \frac{1}{L_i}[\, -S_{iy} \,|\, S_{ix} \,|\, E_{ix}S_{ix} + E_{iy}S_{iy} \,] \begin{bmatrix} a_{Gx} \\ a_{Gy} \\ \ddot{\phi} \end{bmatrix} - \frac{1}{L_i}\big((E_{iy}S_{ix} - E_{ix}S_{iy})\dot{\phi}^2 + 2\dot{L}_i\dot{\alpha}_i\big). \quad (43)$$

Note that, if this equation is written for all four limbs, the first term constitutes $\mathbf{J}_\alpha$, as defined in (25). In order to complete the macro manipulator acceleration analysis it is necessary to derive expressions for the linear accelerations of the center of

mass of each limb. Since in the LAR application, the manipulator is cable driven, it is assumed that the center of mass of each limb is located in the middle of the limbs. Denote the velocity and acceleration of the center of mass of the limbs as $\mathbf{v}_{C_i}$ and $\mathbf{a}_{C_i}$, respectively. The velocity of the center of mass is composed of the tangential and normal components integrated in the following vector equation:

$$\mathbf{v}_{C_i} = \frac{1}{2}\big(\dot{L}_i\hat{\mathbf{S}}_i + \dot{\alpha}_i L_i(\hat{\mathbf{K}} \times \hat{\mathbf{S}}_i)\big). \tag{44}$$

In order to obtain the relation for the acceleration of the center of mass of each limb, differentiate (44) with respect to time:

$$\mathbf{a}_{C_i} = \frac{1}{2}\big((\ddot{L}_i - \dot{\alpha}^2 L_i)\hat{\mathbf{S}}_i + (\ddot{\alpha}_i L_i + 2\dot{L}_i\dot{\alpha}_i)(\hat{\mathbf{K}} \times \hat{\mathbf{S}}_i)\big). \tag{45}$$

Note that the velocity and acceleration of the center of mass of the limbs $\mathbf{v}_{C_i}$ and $\mathbf{a}_{C_i}$ are functions of $\dot{L}_i, \dot{\alpha}_i, \ddot{L}_i$ and $\ddot{\alpha}_i$, whose relation to the macro manipulator velocity and acceleration $\dot{\mathbf{X}}$ and $\ddot{\mathbf{X}}$ are given in (20), (23), (41) and (43), respectively.

3.3.2. Macro–Micro Accelerations

In order to derive expressions for the linear and angular accelerations of the micro limbs, i.e., $\ddot{\ell}_i$ and $\ddot{\beta}_i$, differentiate the vector loop equation (28) with respect to time. Note that $\dot{\hat{\mathbf{s}}}_i = \dot{\beta}_i(\hat{\mathbf{K}} \times \hat{\mathbf{s}}_i)$ and $\dot{\mathbf{e}}_i = \dot{\psi}(\hat{\mathbf{K}} \times \mathbf{e}_i)$. Hence, for $i = 1, 2, \ldots, 4$:

$$\begin{aligned}\mathbf{a}_g + \ddot{\psi}(\hat{\mathbf{K}} \times \mathbf{e}_i) - \dot{\psi}^2\mathbf{e}_i = \mathbf{a}_G + \ddot{\phi}\big(\hat{\mathbf{K}} \times (\mathbf{E}_i + \mathbf{d}_i)\big) - \dot{\phi}^2(\mathbf{E_i} + \mathbf{d_i}) \\ + (\ddot{\ell}_i - \ell_i\dot{\beta}_i^2)\hat{\mathbf{s}}_i + (2\dot{\ell}_i\dot{\beta}_i + \ddot{\beta}_i\ell_i)(\hat{\mathbf{K}} \times \hat{\mathbf{s}}_i).\end{aligned} \tag{46}$$

In order to eliminate $\ddot{\beta}_i$ and get an expression for $\ddot{\ell}_i$, dot multiply both sides by $\hat{\mathbf{s}}_i$ and reorder into:

$$\begin{aligned}\ddot{\ell}_i = \ell_i\dot{\beta}_i^2 + [\, s_{ix} \,|\, s_{iy} \,|\, e_{ix}s_{iy} - e_{iy}s_{ix} \,] \begin{bmatrix} a_{gx} \\ a_{gy} \\ \ddot{\psi} \end{bmatrix} - \dot{\psi}_i^2(\mathbf{e}_i \cdot \hat{\mathbf{s}}_i) \\ - [\, s_{ix} \,|\, s_{iy} \,|\, (E_{ix} + d_{ix})s_{iy} - (E_{iy} + d_{iy})s_{ix} \,] \begin{bmatrix} a_{Gx} \\ a_{Gy} \\ \ddot{\phi} \end{bmatrix} + \dot{\phi}^2(\mathbf{E}_i + \mathbf{d}_i) \cdot \hat{\mathbf{s}}_i.\end{aligned} \tag{47}$$

Cross multiply both side of (46) by $\hat{\mathbf{s}}_i$ to get an expression for $\ddot{\beta}_i$. With some manipulations this leads to:

$$\begin{aligned}\ell_i\ddot{\beta}_i = -2\dot{\ell}_i\dot{\beta}_i + [\, -s_{iy} \,|\, s_{ix} \,|\, \mathbf{e}_i \cdot \hat{\mathbf{s}}_i \,] \begin{bmatrix} a_{gx} \\ a_{gy} \\ \ddot{\psi} \end{bmatrix} - \dot{\psi}^2(e_{iy}s_{ix} - e_{ix}s_{iy}) \\ - [\, -s_{iy} \,|\, s_{ix} \,|\, (\mathbf{E}_i + \mathbf{d}_i) \cdot \hat{\mathbf{s}}_i \,] \begin{bmatrix} a_{Gx} \\ a_{Gy} \\ \ddot{\phi} \end{bmatrix} \\ + \dot{\phi}^2\{(E_{iy} + d_{iy})s_{ix} - (E_{ix} + d_{ix})s_{iy}\}.\end{aligned} \tag{48}$$

In order to complete the macro–micro manipulator acceleration analysis it is necessary to derive expressions for the linear accelerations of the center of mass of the micro limbs. As before, assume that the center of mass of the micro limb is also located at the center of the limbs. Denote the velocity and acceleration of the center of mass of the micro limbs as $\mathbf{v}_{c_i}$ and $\mathbf{a}_{c_i}$, respectively. In order to evaluate these quantities, the absolute position vector of each micro limb $\mathbf{p}_{c_i}$ is written as follows, and by differentiation with respect to time the velocity and acceleration is obtained:

$$\begin{aligned}\mathbf{p}_{c_i} &= \overrightarrow{A_iB_i} + \overrightarrow{B_ia_i} + \frac{1}{2}\ell_i\hat{\mathbf{s}}_i \\ &= L_i\hat{\mathbf{S}}_i + \mathbf{d}_i + \frac{1}{2}\ell_i\hat{\mathbf{s}}_i.\end{aligned}$$

Differentiate with respect to time:

$$\begin{aligned}\mathbf{v}_{c_i} &= \dot{L}_i\hat{\mathbf{S}}_i + L_i\dot{\hat{\mathbf{S}}}_i + \dot{\phi}(\hat{\mathbf{K}}\times\mathbf{d}_i) + \frac{1}{2}\big(\dot{\ell}_i\hat{\mathbf{s}}_i + \ell_i\dot{\beta}_i(\hat{\mathbf{K}}\times\hat{\mathbf{s}}_i)\big) \\ &= \mathbf{v}_G + \dot{\phi}\big(\hat{\mathbf{K}}\times(\mathbf{E}_i+\mathbf{d}_i)\big) + \frac{1}{2}\big(\dot{\ell}_i\hat{\mathbf{s}}_i + \ell_i\dot{\beta}_i(\hat{\mathbf{K}}\times\hat{\mathbf{s}}_i)\big). \qquad (49)\end{aligned}$$

Similarly, the acceleration of the center of mass of micro limb is derived as:

$$\begin{aligned}\mathbf{a}_{c_i} = \mathbf{a}_G &+ \ddot{\phi}\big(\hat{\mathbf{K}}\times(\mathbf{E}_i+\mathbf{d}_i)\big) - \dot{\phi}^2(\mathbf{E}_i+\mathbf{d}_i) \\ &+ \frac{1}{2}\big((\ddot{\ell}_i - \ell_i\dot{\beta}_i^2)\hat{\mathbf{s}}_i + (2\dot{\ell}_i\dot{\beta}_i + \ell_i\ddot{\beta}_i)(\hat{\mathbf{K}}\times\hat{\mathbf{s}}_i)\big). \qquad (50)\end{aligned}$$

4. Dynamic Analysis

The most popular approach used in robotics research to derive the dynamics equation of motion of a parallel manipulator is the Newton–Euler formulation. In this method the free-body diagrams of the limbs and moving platform are considered and the Newton–Euler equations are applied to each isolated body. Using this approach, all constraint forces and moments between the limbs and the moving platform are obtained. In this paper first the dynamic equation of the macro manipulator is derived, and then the dynamic equation for the macro–micro structure is derived and analyzed.

4.1. Macro Manipulator Dynamics

In order to derive the dynamic equation of the macro manipulator, assume for the time being that there exists no micro manipulator, and the reaction forces between the macro and micro manipulator are zero. It is assumed that the moving platform center of mass is located at the center point G, and it has a mass M and moment of inertia I_M. The inertia parameters of the limbs and moving platform are given in Table 1. Furthermore, since in the LAR application the manipulator is cable driven, it is assumed that due to the elongation in the cable length, the mass of the limbs

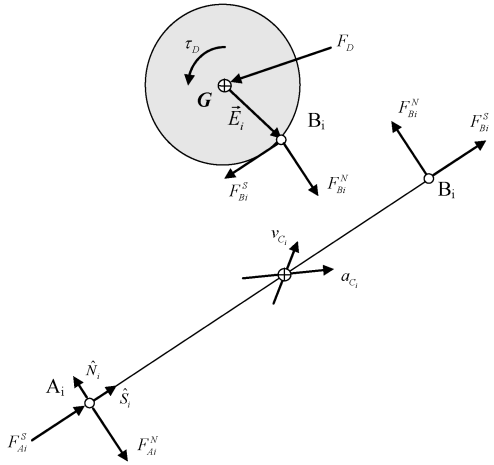

Figure 6. Free-body diagram of the macro manipulator's limb and moving platform.

varies. It is also assumed that the cables are homogeneous, with a circular cross-section, and have a density per unit length of ρ_M. The cables are considered to be in a straight line and modeled as rigid bodies, with varying mass of $M_i = \rho_M L_i$ depending on the cable length. The moment of inertia of the cables also vary and can be calculated assuming that they are slender bars with varying length. The moment of inertia of the cables about the fixed point A_i is given by:

$$I_M^{A_i} = \frac{1}{3} M L_i^2 = \frac{\rho_M}{3} L_i^3. \tag{51}$$

The time derivative of the mass and moment of inertia of each limb is:

$$\dot{M} = \rho_M \dot{L}_i, \qquad \dot{I}_M^{A_i} = \rho_M L_i^2 \dot{L}_i. \tag{52}$$

With these assumptions consider the free-body diagrams of the limbs and the moving platform as illustrated in Fig. 6. The reaction forces at fixed points A_i are illustrated componentwise, and denoted by $F_{A_i}^N$ and $F_{A_i}^S$, in which $\hat{\mathbf{S}}$ is along the limb direction and $\hat{\mathbf{N}}$ is perpendicular to the limb. Similarly, the internal force at points B_i are denoted componentwise as $F_{B_i}^N$ and $F_{B_i}^S$. The velocity and acceleration of the limb center of mass, $\mathbf{v}_{C_i}$ and $\mathbf{a}_{C_i}$, are also shown in Fig. 6. Assume that the only external disturbance force and moment acts on the macro manipulator moving platform, and is denoted by $\mathbf{F}_D = [f_{D_x}, f_{D_y}, \tau_D]^{\mathrm{T}}$.

Let us first derive the equations of motion of the limbs. The Newton–Euler equations for a varying mass system can be written as:

$$\sum \mathbf{F}_{\text{ext}} = \frac{\mathrm{d}}{\mathrm{d}t}(M_i \mathbf{v}_{C_i}) = M_i \mathbf{a}_{C_i} + \dot{M}_i \mathbf{v}_{C_i} \tag{53}$$

$$\sum \mathbf{M}_{A_i} = \frac{\mathrm{d}}{\mathrm{d}t}\left(I_M^{A_i} \dot{\alpha}_i\right) = I_M^{A_i} \ddot{\alpha}_i + \dot{I}_M^{A_i} \dot{\alpha}_i. \tag{54}$$

In which, $\sum F_{\text{ext}}$ is the summation of all external forces acting on the each limb and $\sum M_{A_i}$ denotes the resulting external moments about the fixed point A_i, and the linear velocity and acceleration of each limb at the center of mass, $\mathbf{v}_{C_i}$, $\mathbf{a}_{C_i}$ are given in (44) and (45), respectively. Considering the free body diagram of the limb in Fig. 6, the resulting forces and moments can be determined in vector form as:

$$\big(F^S_{A_i} + F^S_{B_i}\big)\hat{\mathbf{S}}_i + \big(F^N_{B_i} - F^N_{A_i}\big)\hat{\mathbf{N}}_i = M_i \mathbf{a}_{C_i} + \dot{M}_i \mathbf{v}_{C_i} \tag{55}$$

$$F^N_{B_i} L_i = I_M^{A_i} \ddot{\alpha}_i + \dot{I}_M^{A_i} \dot{\alpha}_i. \tag{56}$$

Substituting $\mathbf{v}_{C_i}$ and $\mathbf{a}_{C_i}$ from (44) and (45), and writing (55) componentwise in the $\hat{S}_i$ and $\hat{\mathbf{N}}_i$ direction, with some manipulations this result in:

$$F^S_{A_i} + F^S_{B_i} = \frac{\rho_M}{2}\big(L_i \ddot{L}_i - (L_i \dot{\alpha}_i)^2 + \dot{L}_i^2\big) \tag{57}$$

$$F^N_{B_i} - F^N_{A_i} = \frac{\rho_M}{2}\big(\ddot{\alpha}_i L_i^2 + 3 L_i \dot{L}_i \dot{\alpha}_i\big) \tag{58}$$

$$F^N_{B_i} = \frac{\rho_M}{3}\big(L_i^2 \ddot{\alpha}_i + 3 L_i \dot{L}_i \dot{\alpha}_i\big). \tag{59}$$

Note that in these equations $F^N_{A_i}$ is the pivot reaction force and can be determined by substitution of (59) into (58). By some manipulation:

$$F^N_{A_i} = \frac{\rho_M}{6}\big(L_i^2 \ddot{\alpha}_i + 3 L_i \dot{L}_i \dot{\alpha}_i\big). \tag{60}$$

Furthermore, note that $F^S_{A_i}$ is the actuator forces acting on the limbs and denote it by $F^S_{A_i} = \tau_{A_i}$. Therefore, from (57) and (59) the interacting forces between the limbs and the moving platform, i.e., $F^N_{B_i}$ and $F^S_{B_i}$, are derived, and will be used in the dynamic equation of the moving platform:

$$F^S_{B_i} = \tau_{A_i} - \frac{\rho_M}{2}\big(L_i \ddot{L}_i - (L_i \dot{\alpha}_i)^2 + \dot{L}_i^2\big) \tag{61}$$

$$F^N_{B_i} = \frac{\rho_M}{3}\big(L_i^2 \ddot{\alpha}_i + 3 L_i \dot{L}_i \dot{\alpha}_i\big). \tag{62}$$

Now, the equation of motion of the moving platform is derived, using the free-body diagram depicted in Fig. 6. The Newton–Euler equation of the moving platform is:

$$\sum \mathbf{F}_{\text{ext}} = \mathbf{f}_D - \sum_{i=1}^{4}\big(F^S_{B_i}\hat{\mathbf{S}}_i + F^N_{B_i}\hat{\mathbf{N}}_i\big) = M\mathbf{a}_G \tag{63}$$

$$\sum \mathbf{M}_G = \tau_D \hat{\mathbf{K}} - \sum_{i=1}^{4} \mathbf{E}_i \times \big(F^S_{B_i}\hat{\mathbf{S}}_i + F^N_{B_i}\hat{\mathbf{N}}_i\big) = I_M \ddot{\phi}\hat{\mathbf{K}}. \tag{64}$$

Writing the force equation (63) componentwise, with some manipulation:

$$M\ddot{x}_G - f_{D_x} + \sum_{i=1}^{4}\big(F^S_{B_i} S_{ix} - F^N_{B_i} S_{iy}\big) = 0 \tag{65}$$

$$M\ddot{y}_G - f_{D_y} + \sum_{i=1}^{4}\left(F_{B_i}^S S_{iy} + F_{B_i}^N S_{ix}\right) = 0 \tag{66}$$

$$I_M\ddot{\phi} - \tau_D - \sum_{i=1}^{4}\left(F_{B_i}^S (E_{iy}S_{ix} - E_{ix}S_{iy}) - F_{B_i}^N (\mathbf{E}_i \cdot \hat{\mathbf{S}}_i)\right) = 0. \tag{67}$$

Equations (65)–(67) are the governing equations of motion of the macro manipulator, in which $\mathbf{F}_D = [f_{Dx}, f_{Dy}, \tau_D]^{\mathrm{T}}$ is the disturbance force/torque vector exerted on the moving platform, and the interaction forces between the limbs and the moving platform $F_{B_i}^S$ and $F_{B_i}^N$ are derived from the limb dynamics, and given in (61) and (62), respectively. Furthermore, vectors $\mathbf{E}_i$, and $\hat{\mathbf{S}}_i$, can be found from (17) and (18). Therefore, (65)–(67) can be viewed in an implicit vector form of:

$$\mathbf{f}(\mathbf{X}, \dot{\mathbf{X}}, \ddot{\mathbf{X}}, \mathbf{F}_D, \boldsymbol{\tau}_A) = \mathbf{0}. \tag{68}$$

The use of this equation is 2-fold. The first use of it is to evaluate the actuator forces τ_A needed to produce a prescribed trajectory $\mathbf{X}(t) = [x_G(t), y_G(t), \phi(t)]^{\mathrm{T}}$ in the presence of the disturbance forces and moments $\mathbf{F}_D = [f_{D_x}, f_{D_y}, \tau_D]^{\mathrm{T}}$. Details of the implementation of this application are given in Section 5.1. The most important application of these dynamics equations is in the controller strategies for the system which is elaborated separately in Ref. [19]. Furthermore, the governing equations of motion of the macro manipulator can be implemented for dynamic simulation of the system. In forward dynamic simulation, it is assumed that the actuator forces $\boldsymbol{\tau}_A(t)$ are given and the manipulator motion trajectory $\mathbf{X}(t)$ needs to be determined. As is elaborated in Section 5.2, due to the implicit nature of the dynamic equation, special integration routines capable to integrating implicit differential equations are used for these simulations.

4.2. Macro–Micro Dynamics

In this section the dynamic equation of the macro–micro manipulator is derived using the Newton–Euler formulation. Consider the free-body diagrams of the micro manipulator limbs and moving platform as illustrated in Fig. 7. Similar to the macro manipulator, the reaction forces at points a_i are illustrated componentwise and denoted by $F_{a_i}^n$ and $F_{a_i}^s$, in which, as illustrated, $\hat{\mathbf{s}}$ is along the micro limb direction and $\hat{\mathbf{n}}$ is perpendicular to the micro limb. Similarly, the internal force at points b_i are denoted componentwise as $F_{b_i}^n$ and $F_{b_i}^s$. The velocity and acceleration of the micro limb $\mathbf{v}_{c_i}$ and $\mathbf{a}_{c_i}$ are also shown in this Fig. 7, acting on the center of mass of each micro limb. Assume that an external disturbance force and moment are acting on the micro manipulator moving platform, which is denoted by $\mathbf{F}_d = [f_{d_x}, f_{d_y}, \tau_d]^{\mathrm{T}}$. It is assumed that the moving platform center of mass is located at the center point g, and it has a mass of m and moment of inertia I_m. The inertia parameters of the limbs and moving platform are given in Table 1. Furthermore, similar to the macro manipulator, it is assumed that the micro cables are homogeneous, with a circular cross-section, and have the density per unit length of ρ_m. Hence, the mass of each

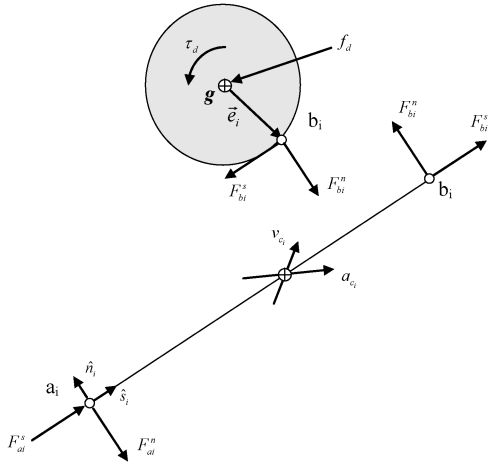

Figure 7. Free-body diagram of the micro manipulator's limb and moving platform.

limb is $m_i = \rho_m \ell_i$. The moment of inertia of the cables also vary and can be calculated by the varying length of the cables. The moment of inertia about the center of mass c_i is given by:

$$I_m^{c_i} = \frac{1}{12} m \ell_i^2 = \frac{\rho_m}{12} \ell_i^3. \tag{69}$$

Hence, the time derivative of mass and moment of inertia of each limb is:

$$\dot{m} = \rho_m \dot{\ell}_i, \qquad \dot{I}_m^{c_i} = \frac{\rho_m}{4} \ell_i^2 \dot{\ell}_i. \tag{70}$$

Similar to the macro manipulator, the Newton–Euler formulation for the micro limb can be written as:

$$\sum \mathbf{F}_{\text{ext}} = \frac{\mathrm{d}}{\mathrm{d}t}(m_i \mathbf{v}_{c_i}) = m_i \mathbf{a}_{c_i} + \dot{m}_i \mathbf{v}_{c_i} \tag{71}$$

$$\sum \mathbf{M}_{c_i} = \frac{\mathrm{d}}{\mathrm{d}t}(I_m^{c_i} \dot{\beta}_i) = I_m^{c_i} \ddot{\beta}_i + \dot{I}_m^{c_i} \dot{\beta}_i, \tag{72}$$

in which $\sum F_{\text{ext}}$ is the summation of all external forces acting on each micro limbs and $\sum M_{c_i}$ denotes the resulting external moments about the center of mass of each limb c_i. Furthermore, the linear velocity and acceleration of each limb at the center of mass, $\mathbf{v}_{c_i}, \mathbf{a}_{c_i}$ are determined before in (49) and (50), respectively. Considering the free body diagram of the limb in Fig. 7, the resulting forces and moments can be determined in a vector form as:

$$\left(F_{a_i}^s + F_{b_i}^s\right)\hat{\mathbf{s}}_i + \left(F_{b_i}^n - F_{a_i}^n\right)\hat{\mathbf{n}}_i = m_i \mathbf{a}_{c_i} + \dot{m}_i \mathbf{v}_{c_i} \tag{73}$$

$$\left(F_{a_i}^n + F_{b_i}^n\right)\frac{\ell_i}{2} = I_m^{c_i} \ddot{\beta}_i + \dot{I}_m^{c_i} \dot{\beta}_i. \tag{74}$$

Substituting $\mathbf{v}_{c_i}, \mathbf{a}_{c_i}$ from (49) and (50), and writing (73) componentwise in the $\hat{s}_i$ and $\hat{\mathbf{n}}_i$ direction, yields the following equations after some manipulations:

$$F^s_{a_i} + F^s_{b_i} = P_{si} + \frac{\rho_m}{2}\big(\ell_i\ddot{\ell}_i - (\ell_i\dot{\beta}_i)^2 + \dot{\ell}_i^2\big) \tag{75}$$

$$F^n_{b_i} - F^n_{a_i} = P_{ni} + \frac{\rho_m}{2}\big(\ell_i^2\ddot{\beta}_i + 3\ell_i\dot{\ell}_i\dot{\beta}_i\big) \tag{76}$$

$$F^n_{a_i} + F^n_{b_i} = \frac{\rho_m}{6}\big(\ell_i^2\ddot{\beta}_i + 3\ell_i\dot{\ell}_i\dot{\beta}_i\big). \tag{77}$$

In which P_{si} and P_{ni} are two intermediate variables as follows:

$$\begin{aligned} P_{si} = {} & \rho_m\big((\ell_i a_{G_x} + \dot{\ell}_i v_{G_x})s_{ix} + (\ell_i a_{G_y} + \dot{\ell}_i v_{G_y})s_{iy} - \dot{\phi}^2\ell_i((\mathbf{E}_i + \mathbf{d}_i)\cdot\hat{s}_i)\big) \\ & + \rho_m\big((\ell_i\ddot{\phi} + \dot{\ell}_i\dot{\phi})((E_{ix} + d_{ix})s_{iy} - (E_{iy} + d_{iy})s_{ix})\big) \end{aligned} \tag{78}$$

$$\begin{aligned} P_{ni} = {} & \rho_m\big((\ell_i a_{G_x} + \dot{\ell}_i v_{G_x})(-s_{iy}) + (\ell_i a_{G_y} + \dot{\ell}_i v_{G_y})s_{ix} \\ & + (\ell_i\ddot{\phi} + \dot{\ell}_i\dot{\phi})((\mathbf{E}_i + \mathbf{d}_i)\cdot\hat{s}_i)\big) \\ & + \rho_m\big(\dot{\phi}^2\ell_i((E_{ix} + d_{ix})s_{iy} - (E_{iy} + d_{iy})s_{ix})\big). \end{aligned} \tag{79}$$

In order to cancel $F^n_{a_i}$, and derive relations for $F^s_{b_i}$ and $F^n_{b_i}$, add (76) and (77) and simplify:

$$F^s_{b_i} = \tau_{a_i} - P_{si} - \frac{\rho_m}{2}\big(\ell_i\ddot{\ell}_i - (\ell_i\dot{\beta}_i)^2 + \dot{\ell}_i^2\big) \tag{80}$$

$$F^n_{b_i} = \frac{1}{2}P_{ni} + \frac{\rho_m}{3}(\ell_i^2\ddot{\beta}_i + 3\ell_i\dot{\ell}_i\dot{\beta}_i), \tag{81}$$

in which, $F^s_{a_i}$ are the actuator forces acting on the micro limbs and are denoted by $F^s_{a_i} = \tau_{a_i}$. The reaction forces $F^n_{a_i}$ can be derived by subtraction of (77) from (76):

$$F^n_{a_i} = \frac{1}{2}P_{ni} + \frac{\rho_m}{6}\big(\ell_i^2\ddot{\beta}_i + 3\ell_i\dot{\ell}_i\dot{\beta}_i\big). \tag{82}$$

Now, the equation of motion of the micro moving platform can be written using the free-body diagram depicted in Fig. 7. The Newton–Euler equations of the micro moving platform are as follows:

$$m\ddot{x}_g - f_{d_x} + \sum_{i=1}^{4}\big(F^s_{b_i}s_{ix} - F^n_{b_i}s_{iy}\big) = 0 \tag{83}$$

$$m\ddot{y}_g - f_{d_y} + \sum_{i=1}^{4}\big(F^s_{b_i}s_{iy} + F^n_{b_i}s_{ix}\big) = 0 \tag{84}$$

$$I_m\ddot{\psi} - \tau_d - \sum_{i=1}^{4}\big(F^s_{b_i}(e_{iy}s_{ix} - e_{ix}s_{iy}) - F^n_{b_i}(\mathbf{e}_i\cdot\hat{\mathbf{s}}_i)\big) = 0. \tag{85}$$

The equation of motion of the macro moving platform is derived next, noting that not only the cable forces $F^S_{B_i}$ and $F^N_{B_i}$, are acting on it, but the macro manipulator interaction forces $-F^s_{a_i}$ and $-F^n_{a_i}$ are present on this platform:

$$M\ddot{x}_G - f_{D_x} + \sum_{i=1}^{4}\left(F^S_{B_i}S_{ix} - F^N_{B_i}S_{iy}\right) + \sum_{i=1}^{4}\left(\tau_{a_i}s_{ix} - F^n_{a_i}s_{iy}\right) = 0 \tag{86}$$

$$M\ddot{y}_G - f_{D_y} + \sum_{i=1}^{4}\left(F^S_{B_i}S_{iy} + F^N_{B_i}S_{ix}\right) + \sum_{i=1}^{4}\left(\tau_{a_i}s_{iy} + F^n_{a_i}s_{ix}\right) = 0 \tag{87}$$

$$\begin{aligned} I_M\ddot{\phi} - \tau_D - \sum_{i=1}^{4}\left(F^S_{B_i}(E_{iy}S_{ix} - E_{ix}S_{iy}) - F^N_{B_i}(\mathbf{E}_i\cdot\hat{\mathbf{S}}_i)\right) \\ - \sum_{i=1}^{4}\left(\tau_{a_i}\left((E_{ix}+d_{ix})s_{iy} - (E_{iy}+d_{iy})s_{ix}\right) + F^n_{a_i}\left((\mathbf{E}_i+\mathbf{d}_i)\cdot\hat{s}_i\right)\right) = 0. \end{aligned} \tag{88}$$

Equations (83)–(88) are the governing equations of motion of the macro–micro manipulator, in which $\mathbf{F}_D = [f_{Dx}, f_{Dy}, \tau_D]^{\mathrm{T}}$ and $\mathbf{F}_d = [f_{dx}, f_{dy}, \tau_d]^{\mathrm{T}}$ are the vectors of disturbance force/torque exerted on the macro and micro moving platforms, respectively. Moreover, the internal forces $F^S_{B_i}$, $F^N_{B_i}$, $F^S_{b_i}$, $F^N_{b_i}$ and $F^n_{a_i}$ are derived in (61), (62), (80), (81) and (82), respectively. Furthermore, the vectors $\mathbf{E}_i$, and $\hat{\mathbf{S}}_i$, are given in (17) and (18), and the vectors $\hat{\mathbf{s}}_i$ and $\mathbf{d}_i$ are given in (29) and (30). Therefore, the set of six inverse dynamic equations of the macro–micro manipulator, i.e., (83)–(88), can be written in an implicit vector form of:

$$\mathbf{f}(\mathbf{x}, \dot{\mathbf{x}}, \ddot{\mathbf{x}}, \mathbf{X}, \dot{\mathbf{X}}, \ddot{\mathbf{X}}, \mathbf{F}_d, \mathbf{F}_D, \boldsymbol{\tau}_a, \boldsymbol{\tau}_A) = \mathbf{0}. \tag{89}$$

As explained for the macro manipulator, this vector equation can be used directly for an inverse dynamics control scheme or for forward dynamic simulation of the system. The details of implementation and the numerical simulation results are reported in the next section.

5. Implementation of the Formulations

As explained earlier, the dynamic equation of the macro–micro manipulator can be used in two applications. In the first application, which is simulated in Section 5.1, the Cartesian and actuator forces required to produce a prescribed trajectory for the system are determined numerically. The most important use of this type of implementation of dynamics equations is in the proposed controller strategies for the system which is elaborated in detail in Ref. [19]. The second application of the dynamic equations of the macro–micro manipulator is the direct dynamic simulation of the system. In this case it is assumed that the actuator forces are given and the manipulator motion is to be determined. Due to the implicit nature of the dynamic

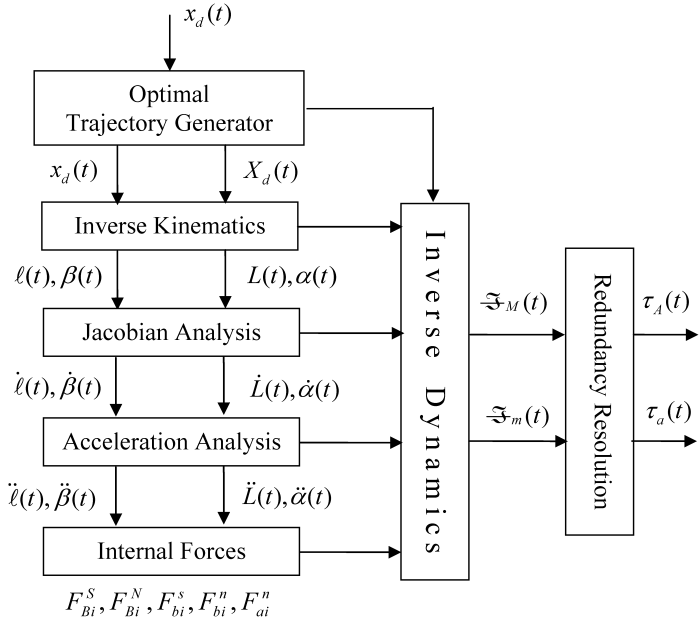

Figure 8. Flowchart of the inverse dynamics implementation sequence.

equations, the usual numerical integration routines such as the Runge–Kutta methods [20] cannot be used to solve this problem. As it is elaborated in Section 5.2, special integration routines, which are able to integrate implicit differential equations, are used for these simulations.

5.1. Inverse Dynamics Simulation

In inverse dynamic simulations, it is assumed that the trajectory of the macro–micro manipulator is given and the actuator forces required to generate such trajectories in the presence of disturbances are to be determined. Due to the implicit nature of the dynamic equations, as illustrated in Fig. 8, the inverse dynamic formulation is implemented in the following sequence.

The first step is the optimal trajectory generation of the macro–micro manipulator. Macro–micro structures such as the one being investigated in this paper are kinematically redundant. In order to generate complete planar motion for the micro moving platform, only the micro or macro actuators are sufficient. However, in order to obtain very accurate positioning, a set of complete actuation levels is redundantly added to the manipulator design. Although the availability of the extra d.o.f. can provide dexterous motion of the micro moving platform, proper utilization of this redundancy is an important issue to be considered. For a macro–micro manipulator, the desired trajectory of the final micro manipulator $\mathbf{x}_d$ is usually given, and due to the inherent kinematic redundancy of macro–micro manipulator, infinitely many self motion trajectories for the macro manipulator location $\mathbf{X}_d$, and joint variables $\dot{\boldsymbol{\ell}}$ and $\dot{\mathbf{L}}$ exist to perform the maneuver required for the micro manipulator. In

Ref. [21] an analysis based on macro–micro Jacobian matrices is performed to design optimal trajectories for the macro and micro manipulators. Two scenarios are examined in which in the first case the relative motion for the micro manipulator is minimized, while in the second case for some singular configuration the optimal trajectory is designed to maximize the manipulability measure of the macro–micro manipulator. As shown in Ref. [21], for trajectories away from singular configurations, the optimal trajectory which minimized the micro manipulator motion is $\mathbf{x}_d(t) = \mathbf{X}_d(t)$. However, in cases where the singularity can be experienced the singularity avoidance optimization method can be used. For the sample trajectory of the manipulator which is illustrated below in Fig. 16, the first case is considered.

The next step is to solve the inverse kinematics of the manipulator and to find $\mathbf{L}(t), \boldsymbol{\alpha}(t), \boldsymbol{\ell}(t)$ and $\boldsymbol{\beta}(t)$, using (8), (9), (12) and (14), respectively. Then the manipulator Jacobian matrices $\mathbf{J}_M$, $\mathbf{J}_m$ and $\mathbf{J}_t$ are calculated through (21), (33) and (37), respectively. This implies that $\dot{\mathbf{L}}(t), \dot{\boldsymbol{\alpha}}(t), \dot{\boldsymbol{\ell}}(t)$ and $\dot{\boldsymbol{\beta}}(t)$, are calculated as well. Next the accelerations are evaluated using the acceleration analysis equations (41), (43), (47) and (48). Finally, all the interaction forces, i.e., $F^S_{B_i}, F^N_{B_i}, F^s_{b_i}, F^n_{b_i}$ and $F^n_{a_i}$, are computed from (61), (62), (80), (81) and (82), and are substituted in the governing inverse dynamic equations of the macro–micro manipulator. Let us denote the resulting Cartesian force applied to the macro and micro moving platforms $\mathcal{F}_t$. In this definition $\mathcal{F}_t = [\mathcal{F}_M, \mathcal{F}_m]^{\mathrm{T}}$ is the resulting Cartesian force applied to the macro and micro manipulator moving platform, and calculated from the summation of all inertial and external forces excluding the actuator torques $\boldsymbol{\tau}_t = [\boldsymbol{\tau}_A, \boldsymbol{\tau}_a]^{\mathrm{T}}$ in the dynamic equations (83)–(88). Hence, $\mathcal{F}_t = \mathbf{J}_t^{\mathrm{T}} \boldsymbol{\tau}_t$ is the projection of the actuator forces on the moving platform and can be uniquely determined from the dynamic equations by excluding the actuator forces from the dynamic equations. If the manipulator has no redundancy in actuation, the Jacobian matrix, $\mathbf{J}_t$, is squared and the actuator forces can be uniquely determined by $\boldsymbol{\tau}_t = \mathbf{J}_t^{-\mathrm{T}} \mathcal{F}_t$, provided that $\mathbf{J}_t$ is nonsingular. For redundant manipulators, however, there are infinity many solutions for $\boldsymbol{\tau}_t$ to be projected into $\mathcal{F}_t$. The simplest solution would be a minimum norm solution, which is found from the pseudo-inverse of $\mathbf{J}_t^{\mathrm{T}}$, by $\boldsymbol{\tau}_t = \mathbf{J}_t^{T^\dagger} \mathcal{F}_t$. This solution is implemented in the simulation studies reported in this section. Other optimization techniques can be used to find the actuator forces projected from $\mathcal{F}_t$ subject to more detailed manipulator constraints, whose details are reported in Ref. [19].

The inverse dynamics of the macro–micro manipulator are simulated for two cases. In the first set of simulation results the inverse dynamic solution is computed in absence of any disturbance forces $\mathbf{F}_D = \mathbf{F}_d = \mathbf{0}$. The simulation results are illustrated in Figs 9–12. Typical third-order polynomial trajectories for the manipulator are considered in these simulation, as depicted in Fig. 16. The Cartesian forces at the macro moving platform, $\mathcal{F}_M = [\mathcal{F}_X, \mathcal{F}_Y, \mathcal{F}_\phi]^{\mathrm{T}}$, are illustrated with the solid line in Fig. 9. As is seen, the Cartesian forces have a similar pattern to the desired trajectory accelerations, which are linear for the cubic trajectories. In order to compare the contribution of the moving platform inertia compared to that of the limb inertial terms, the moving platform inertia forces are depicted by the dashed line in

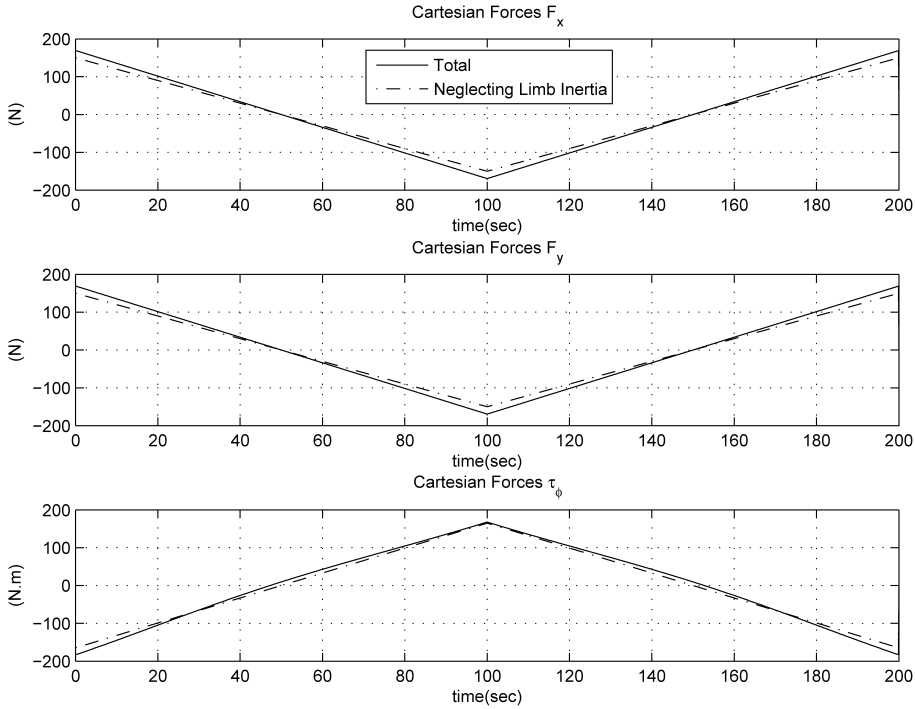

Figure 9. Cartesian forces of the macro manipulator $\mathcal{F}_M$: the total force (solid) and neglecting limb inertia (dashed).

Fig. 9. As is seen, the effect of the limb inertia forces are about 10% of the total for such a trajectory. Similarly, the actuator forces of the macro manipulator, with the indication of moving platform inertia contributions, are illustrated in Fig. 10. It is observed that since the manipulator moves in positive x and y directions, the actuator forces of the first and third limbs are dominant. Figures 11 and 12 illustrate the Cartesian and actuator forces of the macro manipulator, in a similar fashion as that in the macro manipulator. It is observed that the contribution of the micro limb dynamics is negligible.

In the second set of simulations, the effect of disturbance forces acting on the system is analyzed. A set of experimental disturbance forces is considered in this study to be applied to the macro–micro manipulator. The disturbance forces due to the wind turbulence are measured in a one-third scale prototype of the multi-tethered aerostat subsystem [7], which is implemented in Penticton. The horizontal measured forces are scaled-up by a factor of 27 and applied on the macro manipulator, in order to replicate the behavior of the full-size system. The exerted disturbance forces on the macro manipulator are given with the dotted line in Fig. 13. The Cartesian and actuator forces of the macro manipulator in presence of such disturbance are depicted in Figs 13 and 14, respectively. As is seen, the contribution of the disturbance force into the total Cartesian forces on the manipulator is dominant.

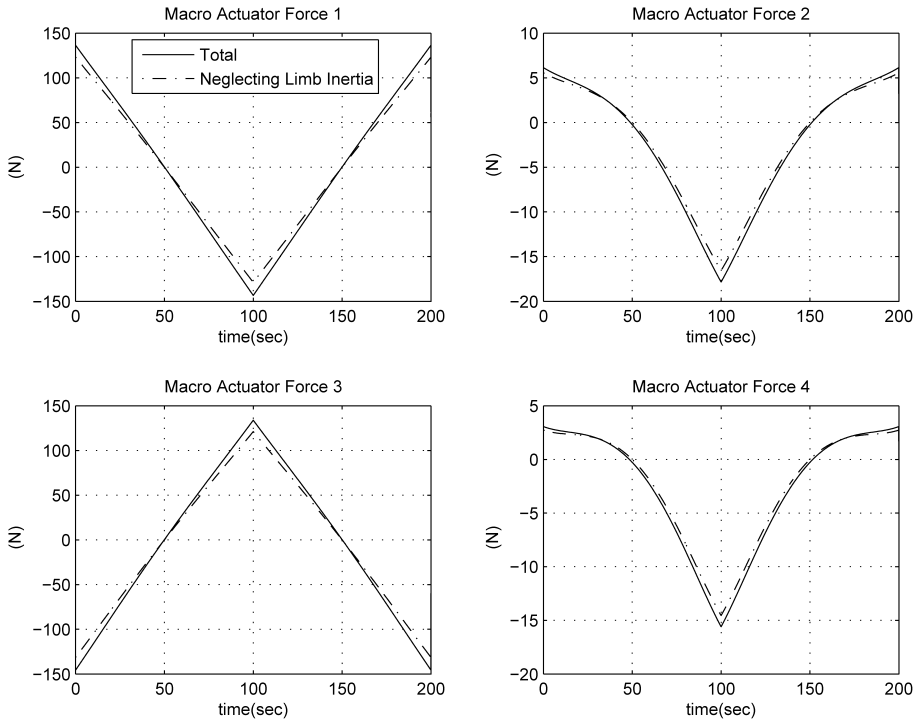

Figure 10. Actuator forces of the macro manipulator $\boldsymbol{\tau}_A$: the total force (solid) and neglecting limb inertia (dashed).

Comparing the values of forces in Figs 9 and 13, it is observed that the total inertial forces contribute about 10% of the total forces for such typical disturbance. Noting that the limb dynamics contributes only 10% of inertial forces, it can be neglected in the full simulation of the system in the presence of external disturbances.

5.2. Forward Dynamics Simulation in the Closed Loop

As explained before, the dynamic equations of motion of the macro–micro manipulator can be used for forward dynamic simulation of the system. In this case it is assumed that the actuator forces are given and the manipulator motion is to be determined. Due to the implicit nature of the dynamic equation, usual numerical integration routines such as the Runge–Kutta methods [20] cannot be used to solve the problem. However, a special integration routine (`ode15i` function of Matlab), which is able to integrate implicit functions, can be used for dynamic simulations. The Block diagram of forward dynamic simulation in the closed-loop form is given in Fig. 15. As it is illustrated in this block diagram, the inverse dynamic equations of motion, i.e., (83)–(88), are the main equations to be integrated using an implicit integration routine. These equations, written in vector form in (89), are integrated numerically using a repeating algorithm with respect to time, given the function input arguments, $\mathbf{x}, \dot{\mathbf{x}}, \mathbf{X}, \dot{\mathbf{X}}, \mathbf{F}_d, \mathbf{F}_D, \boldsymbol{\tau}_a$ and $\boldsymbol{\tau}_A$, and the initial

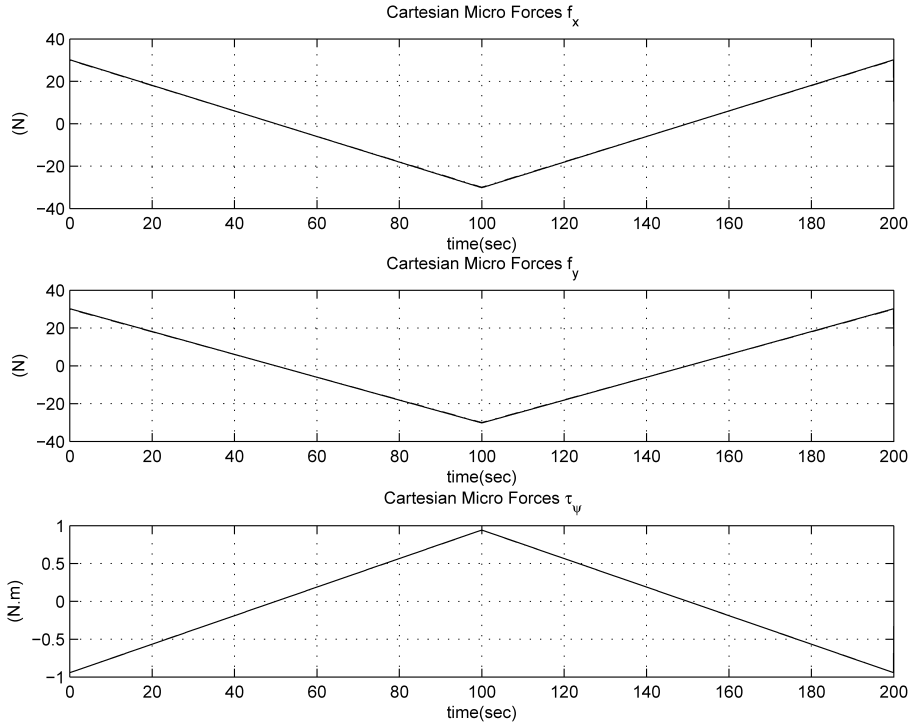

Figure 11. Cartesian forces of the micro manipulator, $\mathcal{F}_m$.

conditions for the function states $\mathbf{x}(0), \dot{\mathbf{x}}(0), \mathbf{X}(0)$ and $\dot{\mathbf{X}}(0)$. The experimental disturbance forces $\mathbf{F}_d$ and $\mathbf{F}_D$, explained in the previous section, are used in dynamic simulation of the macro–micro manipulator in hand. Furthermore, as shown in Fig. 15, pseudo-inverse of the total Jacobian, $\mathbf{J}_t^{\dagger}$, is used as the redundancy resolution scheme. The controllers used in these simulations are decentralized PD controllers for macro and micro manipulators, in which the gains are tuned such that, despite the saturation limit in actuator efforts, the required tracking performance is achieved. For a typical actuator saturation limit of 5 KN for the macro manipulator and 50 N for the micro manipulator actuators, the PD gains used in the simulations are $K_P = 10^6 \cdot I_3$, $K_D = 10^8 \cdot I_3$, $K_p = 10^5 \cdot I_3$ and $K_d = 10^7 \cdot I_3$, in which the capital indices are used for macro manipulator gains and I_3 is the 3×3 identity matrix.

The closed-loop tracking performance of the macro–micro manipulator is illustrated in Figs 16 and 17. The desired trajectory is as in previous simulations and is illustrated in Fig. 16. As seen in Fig. 16 the desired and final closed-loop motion of the system is not distinguishable. As seen in more detail in Fig. 17, a decentralized PD controller for the macro and micro manipulators is capable of reducing the tracking errors to less than 1 mm in position and less than 0.2° in orientation for the macro manipulator. Moreover, due to the macro–micro structure of the manipulator

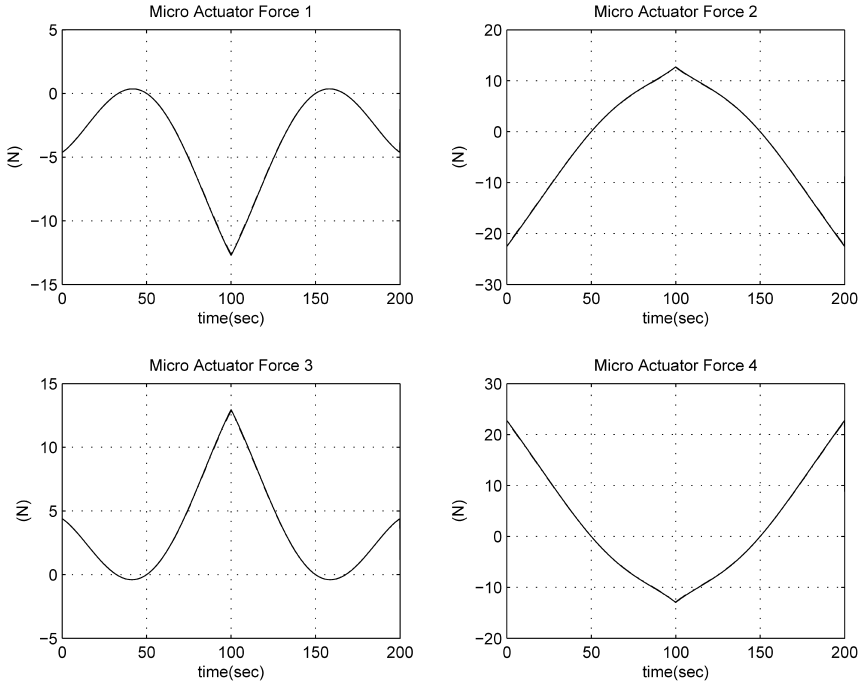

Figure 12. Actuator forces of the micro manipulator, $\boldsymbol{\tau}_a$.

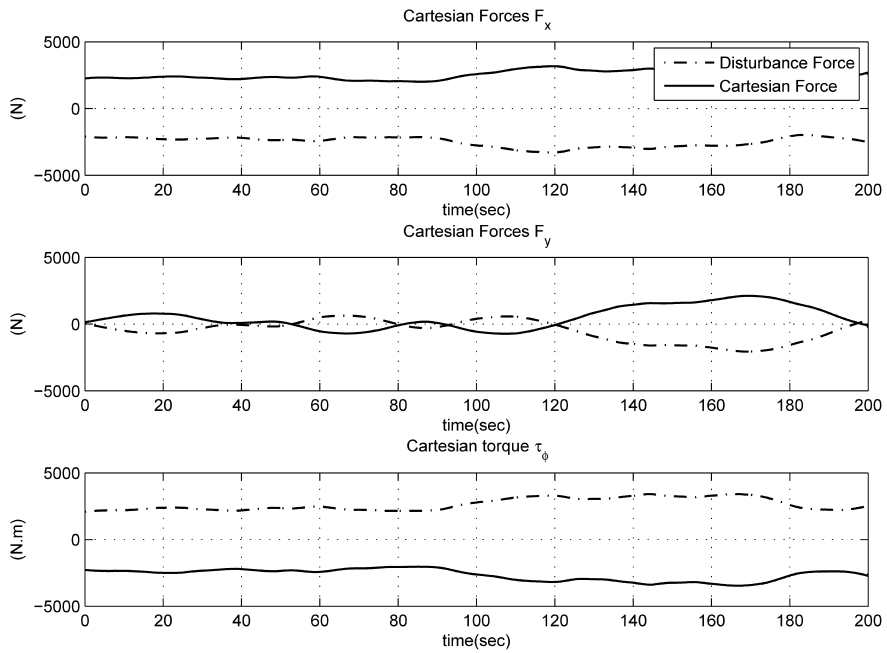

Figure 13. Cartesian forces of the macro manipulator $\mathcal{F}_M$, in the presence of empirical disturbance $\mathbf{F}_d$.

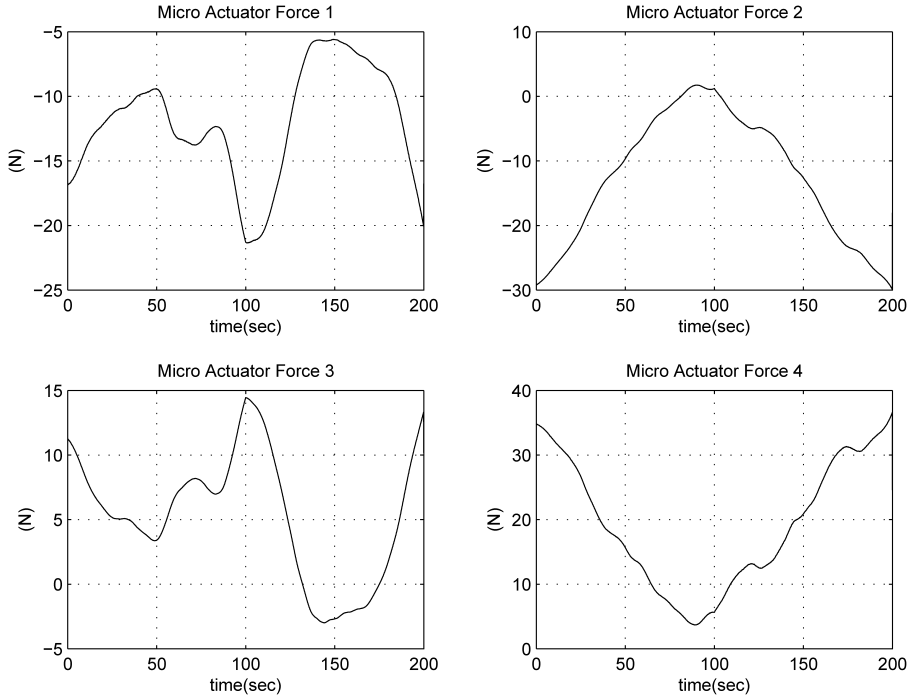

Figure 14. Actuator forces of the macro manipulator $\boldsymbol{\tau}_A$, in the presence of empirical disturbance $\mathbf{F}_d$.

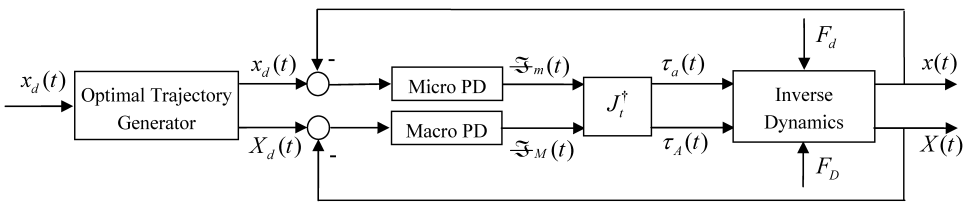

Figure 15. Block diagram of PD control.

the final tracking error of the system is reduced to less than 0.1 mm in position and 0.02° in orientation in the presence of experimentally measured disturbance forces acting on the system. This results confirms the original idea of using the macro–micro structure for extra accurate positioning devices and shows that when using this structure the tracking errors can be reduced to 1/10th of that in the first stage of the macro–micro structure. It should be noted that, although the desired trajectories in the x- and y-directions are considered identical, but because of the desired orientation ϕ_d, which is negative in this typical trajectory, the order of error in the y-direction is less than that in the x-direction. However, this is not a general case for all trajectories, i.e., if the orientation direction is changed, the order of the positioning error in the x-direction becomes less than that in the y-direction.

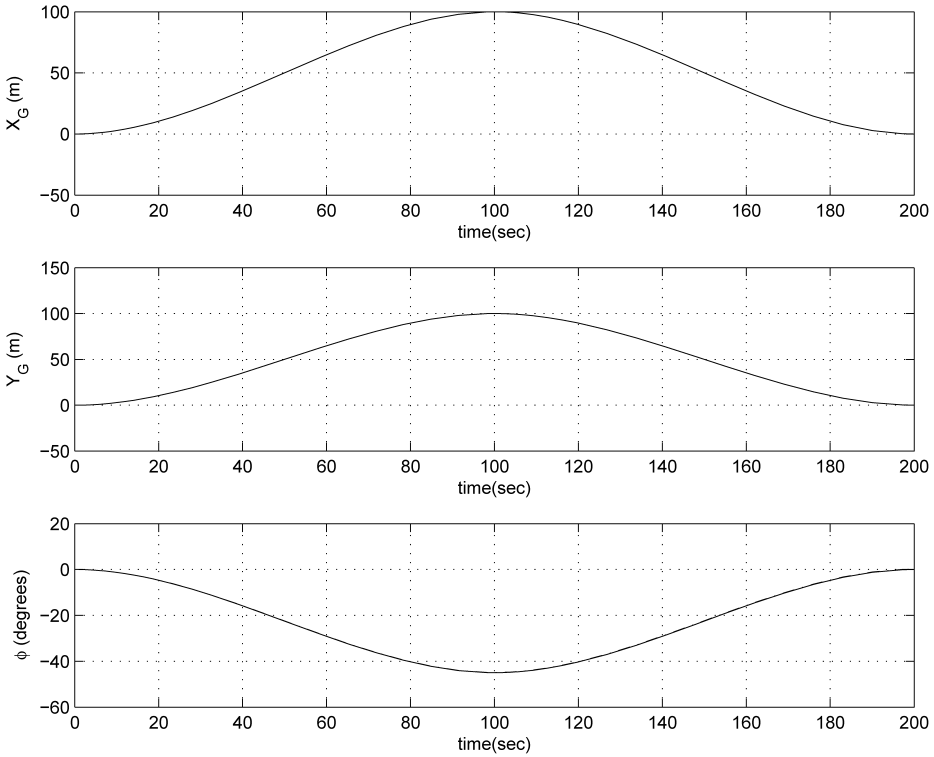

Figure 16. Closed-loop tracking performance of the macro–micro manipulator.

In order to examine the effect of disturbances on the actuator forces, Fig. 18 illustrates the macro actuate force. As seen in Fig. 18, the macro actuator effort is well below the empirical saturation limit of 5 kN. The simulation results verify the fact that the decentralize PD controllers are able to provide the desired tracking performance in the closed loop. The redundancy resolution technique used in here, however, is very simple and, as shown in Ref. [19], it can be developed optimally, in order to guarantee that the cable-driven actuators are in tension in all configurations of the macro–micro maneuvers.

6. Conclusions

In this paper the kinematic and dynamic analysis of a macro–micro parallel manipulator is studied in detail. The analyzed manipulator is a planar version adopted from the structure of the LAR, the Canadian design of next-generation giant radio telescopes. In the LAR design the telescope receiver package is supported by a tension structure consisting of multiple long tethers and a helium-filled aerostat. The positioning structure of the receiver is designed as a macro–micro manipulator, in which at both the macro and micro levels two redundantly actuated cable-driven parallel manipulators are used and both manipulators experience 6-d.o.f. motion

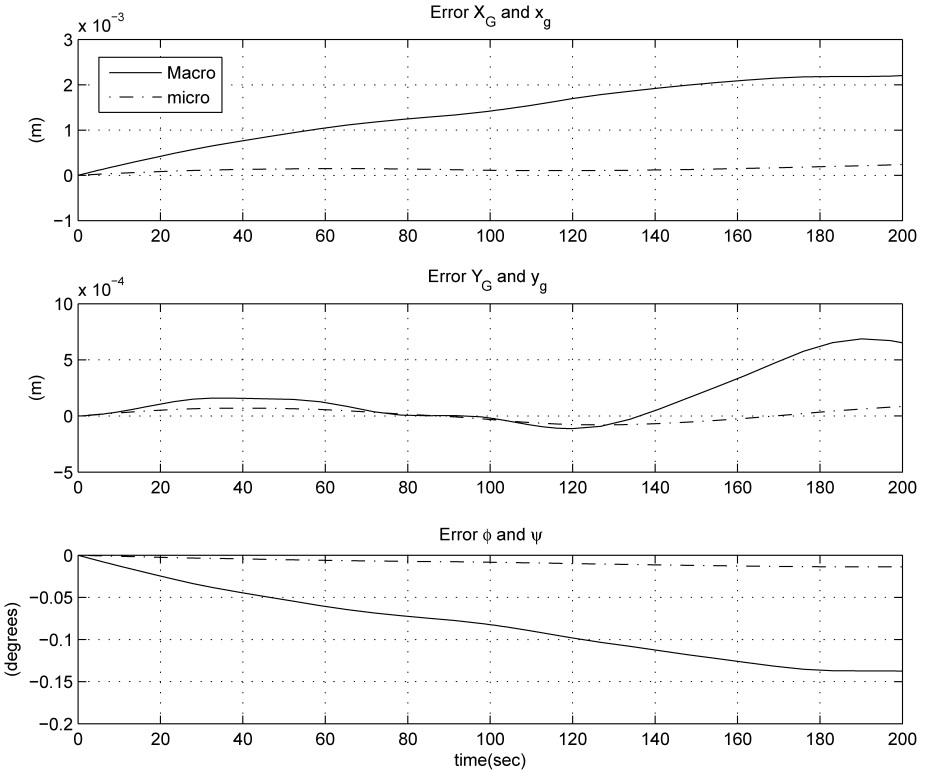

Figure 17. Macro and micro tracking errors: macro (solid) and micro (dashed).

in space. The planar structure used in this paper is a simplified version of the LAR design, in which the two important features of the main mechanism, i.e., the macro–micro structure and actuator redundancy, are preserved in a planar structure. This structure is composed of two 3-d.o.f. parallel redundant manipulators at the macro and micro level, both actuated by cables. A thorough analysis of the kinematics and dynamics of the described macro–micro parallel manipulator has been performed, and some closed-loop control topologies are proposed and simulated for this system. In this paper the kinematic and dynamic analysis of this system is presented. It is shown that a unique closed-form solution to the inverse kinematic problem of such a structure exists. Moreover, the Jacobian and acceleration analysis for the macro–micro manipulator is reported. Next, the dynamic equation of motion of the macro–micro manipulator is derived using the Newton–Euler formulation. Then, the dynamic equations of the system are used in two sets of simulations. First, the inverse dynamic simulations are presented, in which the required actuator torques required to generate a prescribed trajectory are computed. It is shown that for a typical trajectory, the limb inertial forces contributes only in 10% of the dynamic forces and the total dynamic forces contribute only 10% of external forces in the presence of some experimentally measured disturbance forces. Finally, the inverse

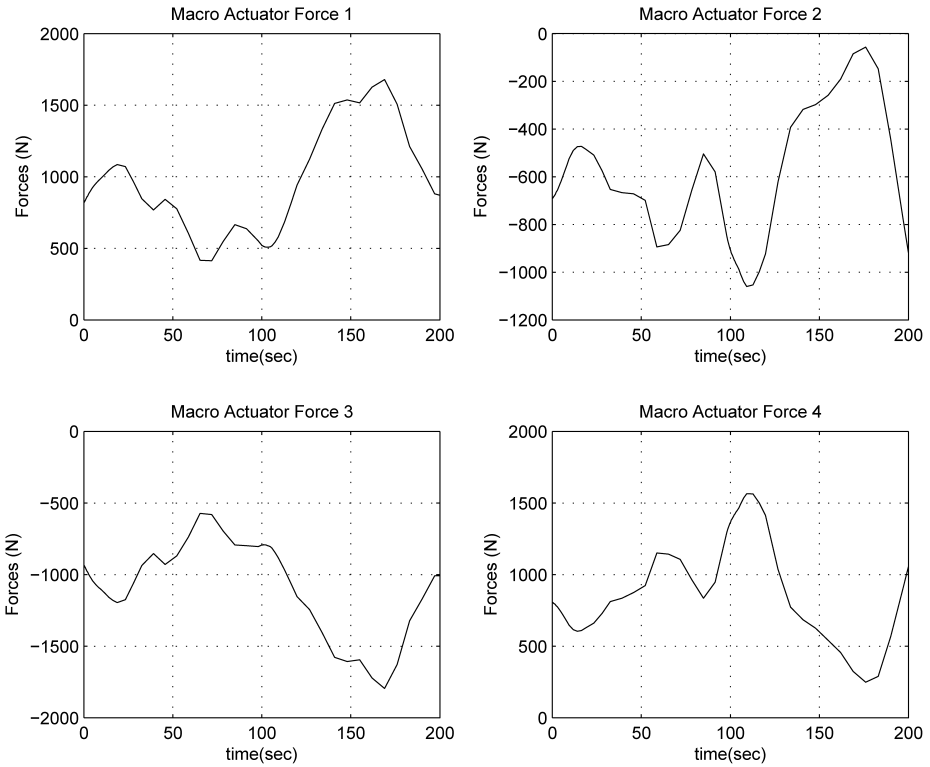

Figure 18. Closed-loop actuator forces of the macro manipulator, $\boldsymbol{\tau}_A$.

dynamic equations are used in a special implicit integration routine in order to simulate the dynamic behavior of the system in closed-loop form and in the presence of disturbances. It is shown that, for a typical trajectory and in the presence of experimentally measured disturbance forces, using the macro–micro structure will increase the positioning accuracy of the system 10 times more than that for the first stage of the macro–micro structure.

Acknowledgements

The authors gratefully acknowledge the financial support received from the K. N. Toosi University of Technology, and PBEEE Quebec Visiting Scientist Award, and the Natural Sciences and Engineering Research Council of Canada.

References

1. D. H. Chaubert, A. O. Boryssenko, A. van Ardenne, J. G. Bij de Vaate and C. Craeye, The Square Kilometer Array (SKA) Antenna, in: *Proc. IEEE Int. Symp. on Phased Array Systems and Technology*, Boston, MA, pp. 351–358 (2003).

2. M. V. Ivashina, A. van Ardenne, J. D. Bregman, J. G. B. de Vaate and M. van Veelen, Activities for the square kilometer array (SKA) in Europe, in: *Proc. Int. Conf. on Antenna Theory and Techniques*, Boston, MA, pp. 633–636 (2003).
3. A. van Ardenne, Concepts of the square kilometre array and toward the new generation radio telescopes, in: *Proc. IEEE Int. Symp. of the Antennas and Propagation Society*, Tokyo, pp. 158–161 (2000).
4. B. Carlson, L. Bauwens, L. Belototski, E. Cannon, Y. Deng, P. Dewdney, J. Fitzsimmons, D. Halliday, K. Krschner, G. Lachapelle, D. Lo, P. Mousavi, M. Nahon, L. Shafai, S. Stiemer, R. Taylor and B. Veidt, The large adaptive reflector: a 200-m diameter, wideband, cm-wave radio telescope, in: *Radio Telescopes: Proc. SPIE Meeting 4015*, Bellingham, WA, pp. 33–44 (2000).
5. P. Dewdney, M. Nahon and B. Veidt, The large adaptive reflector: a giant radio telescope with an areo twist, *Can. Aeronaut. Space J.* **48**, 239–250 (2002).
6. P. Mousavi, L. Shafai, B. Veidt and P. Dewdney, Feed-reflector design for large adaptive reflector antenna (LAR), *IEEE Trans. Antennas Propagat.* **49**, 1142–1154 (2001).
7. C. Lambert, A. Saunders, C. Crawford and M. Nahon, Design of a one-third scale multi-tethered aerostat system for precise positioning of a radio telescope receiver, in: *Proc. CASI Flight Mechanics and Operations Symp.*, Montreal, pp. 1–12 (2003).
8. C. Gosselin, Parallel computational algorithms for the kinematics and dynamics of planar and spatial parallel manipulators, *Trans. ASME J. Dyn. Syst. Meas. Control* **118**, 22–28 (1996).
9. N. Dasgupta and T. S. Mruthyunjaya, A Newton–Euler formulation for the inverse dynamics of the Stewart platform manipulator, *Mechanism and Machine Theory* **33**, 1135–1152 (1998).
10. C. C. Nguyen and F. J. Pooran, Dynamic analysis of a 6 DOF CKCM robot end-effector for dual-arm telerobot systems, *Robotics Auton. Syst.* **5**, 377–394 (1989).
11. G. Lebret, K. Liu and F. L. Lewis, Dynamic analysis and control of a Stewart platform manipulator, *J. Robotic Syst.* **10**, 629–655 (1993).
12. Jiegao Wang and C. M. Gosselin, A new approach for the dynamic analysis of parallel manipulators, *Multibody Syst. Dyn.* **2**, 317–334 (1998).
13. J. McPhee, P. Shi and J. C. Piedboeuf, Dynamics of multibody systems using virtual work and symbolic programming, *Math. Comp. Model. Dyn. Syst.* **8**, 137–155 (2002).
14. L. T. Wang and C. C. Chen, On the dynamic analysis of general parallel robotic manipulators, *Int. J. Robotics Automat.* **9**, 81–87 (1994).
15. M.-J. Liu, C.-X. Li and C.-N. Li, Dynamics analysis of the Gough–Stewart platform manipulator, *IEEE Trans. Robotics Automat.* **16**, 94–98 (2000).
16. S.-H. Lee, J.-B. Song and D. Hong, Position control of a Stewart platform using inverse dynamics control with approximate dynamics, *Mechatronics* **13**, 605–619 (2003).
17. H. Cheng, Y.-K. Yiu and Z. Li, Dynamics and control of redundantly actuated parallel manipulators, *IEEE/ASME Trans. Mechatron.* **8**, 483–491 (2003).
18. H. D. Taghirad and M. Nahon, Dynamic analysis of a redundantly actuated parallel manipulator: a virtual work approach, in: *Proc. Iranian Conf. on Electrical Engineering*, Tehran, vol. 3, pp. 54–60 (2007).
19. H. D. Taghirad and M. Nahon, Redundancy resolution and inverse dynamics control of a macro–micro redundantly actuated parallel manipulator, *Int. J. Robotics Syst.*, submited (2008).
20. L. F. Shampine, *Numerical Solution of Ordinary Differential Equations*. Chapman and Hall, New York, NY (1994).
21. H. D. Taghirad and M. Nahon, Kinematic analysis of a macro–micro redundantly actuated parallel manipulator, *Adv. Robotics* **22**, 657–687 (2008).

About the Authors

Hamid D. Taghirad received his BS degree in Mechanical Engineering from Sharif University of Technology, Tehran, Iran, in 1989, his ME in Mechanical Engineering, in 1993, and his PhD in Electrical Engineering, in 1997, both from McGill University, Montreal, Canada. He is currently an Associate Professor with the Electrical Engineering Department, and the Director of the Advanced Robotics and Automated System, ARAS Research Center at K. N. Toosi University of Technology, Tehran, Iran. He was appointed as the Director of the Office of International Scientific Cooperation of the university in 2007. He is a Senior Member of the IEEE, and his publications include two books, and more than 90 papers in international Journals and conference proceeding. His research interests are robust and nonlinear control applied on robotic systems.

Meyer A. Nahon received the BAS degree in Mechanical Engineering from Queen's University, Kingston, ON, Canada, the MAS degree in Aerospace Engineering from the University of Toronto, Toronto, ON, and the PhD degree in Mechanical Engineering from McGill University, Montreal, QC, Canada. He was an Assistant and Associate Professor of Mechanical Engineering with the University of Victoria, Victoria, BC, Canada, from 1991 to 2001, and since then, he has been an Associate Professor of Mechanical Engineering at McGill University. His present research deals with various aspects of robotics, including dynamics and control of aerial and undersea vehicles; mechanics of parallel mechanisms; and distance determination algorithms. He is an Associate Fellow of the AIAA and the Canadian Aeronautics and Space Institute (CASI). He has received awards from the AIAA and CASI for his work on flight simulator motion systems and on space-based robotics.